APPLICATION OF NEURAL NETWORKS TO AEROMECHANICS PROBLEMS

Sesi Kottapalli
Aeromechanics Branch
Army/NASA Rotorcraft Division
NASA Ames Research Center
Moffett Field, California
USA

ABSTRACT

Recent research on applying neural networks to rotorcraft aeromechanics problems is discussed. The present neural network aeromechanics applications cover the following technical areas: 1) identification and control and 2) test data validation (including formulation and implementation of a wind correction procedure for outdoor hover performance test data). The first aeromechanics application of neural networks is identification and control of advancing-side, blade-vortex-interaction (BVI) noise and vibratory hub loads. The present closed loop neural network controller successfully achieved simultaneous reductions of 5 dB in the advancing side noise and 54% in the vibratory hub loads. Compared to a one-step deterministic controller, the present neural network controller was more robust. The second application is experimental data validation including both hover and forward flight test data. The networks accurately captured tilt-rotor performance at steady operating conditions and showed that the wind tunnel forward flight performance test data were generally of high quality. The wind correction procedure used full-scale XV-15 tilt-rotor outdoor hover performance data obtained from a NASA Ames Outdoor Aerodynamic Research Facility test. The present wind corrections procedure, based on a well-trained neural network, captured physical trends present in the outdoor hover test data that had been missed by the existing, momentum-theory-based method. Overall, the present study concluded that neural networks are very useful in solving aeromechanics problems.

NOTATION

A	Rotor disc area, πR^2, m^2	C_Q	Rotor torque coefficient, Torque/ρARV^2_{tip}
A_2	Experimental 2P control amplitude input, deg	FM	Figure of merit, $FM = 0.707 C_T^{3/2}/C_Q$
A_m	Amplitude of mP IBC input, deg		
ASNM	Advancing side noise metric, dB	FM-delta	Figure of merit delta, difference between test and zero wind figures of merit, Δ_T
a	Speed of sound, m/s		
BL-SPL	Band-limited sound pressure level, dB	FM_{TEST}	Figure of merit, test
BVI	Blade vortex interaction	FM_{ZW}	Figure of merit, neural network representation of test figure of merit for "zero wind" conditions
c	Blade chord		
		HHC	Higher Harmonic Control

i	Blade number; $i=1$ implies $\psi=0$ for blade at helicopter tail	W_{ASNM}	Weight for $ASNM^2$ in objective function J
IBC	Individual Blade Control	$[W_Z]$	Weighting matrix, of 11 x 11 (noise and vibratory hub loads)
INNC	Inverted neural network for control		
J	Noise and vibratory hub loads objective function, weighted sum of the squares of ASNM and VHLM	$\{z\}$	Vector of measured vibratory hub loads and noise metric, of size 11 x 1
		Zero wind	Refers to wind with $V_w < 0.5$ m/s
m	Harmonic number for IBC input	α_s	Rotor shaft angle, positive nose up, deg
MIMO	Multiple-input, multiple-output		
MISO	Multiple-input, single-output	Δ_T	Symbol for FM-delta
M_{tip}	Rotor hover tip Mach number, V_{tip}/a	Θ_0	Collective angle, deg
n	Parameter defining J_T, $J_T = J_{ND}^n$	$\{\theta\}$	Vector of 2P blade pitch inputs, of size 2 x 1
N_b	Number of blades	$\{\theta^*\}$	Vector of optimal 2P blade pitch inputs, of size 2 x 1
OARF	Outdoor Aerodynamic Research Facility	θ_{im}	IBC contribution to blade pitch, m'th harmonic for i'th blade
R	Rotor radius, m		
RBF	Radial-basis function	μ	Advance ratio
SIMO	Single-input, multiple-output	Φ_2	Experimental 2P control phase input, deg
SISO	Single-input, single-output	$\Phi_{2N,i}$	Neural network controller 2P control phase input for the i'th iteration, deg
SPL	Sound pressure level, dB		
$[T]$	Transfer-function matrix, 11 x 2 (noise and vibratory hub loads)	ρ	Air density, kg/m³
		σ	Rotor solidity, $N_b c/\pi R$
V	Wind tunnel airspeed, knots	ψ	Rotor azimuth angle, deg
V_{tip}	Rotor tip speed, ΩR, m/s	ψ_w	Wind direction relative to rotor axis
V_w	Atmospheric wind speed, m/s		
VHLM	Vibratory hub loads metric. Made up of five equally-weighted, 4P hub loads components	Ω	Rotor rotational speed, rad/sec

INTRODUCTION

The application of neural networks to rotorcraft aeromechanics is still new. The aeromechanics problems that were considered in the present study for "solution" using neural networks are listed as follows: 1) identification and control and 2) test data validation (including a wind correction procedure for outdoor hover performance test data). For each of these problems, neural-network-based techniques are attractive, nonlinear methods of solution. Neural networks do not necessarily require large amounts of computational resources. Additionally, they appear easy to apply and understand.

IDENTIFICATION AND CONTROL

Introduction

The development and implementation of a robust active control system for helicopter aeromechanics must include a method for accurate identification of aircraft parameters and a robust scheme to generate optimal control inputs to best realize a set of objective functions. Specifically, for the aeromechanic problem investigated in this paper, the controller's task would be to first, identify the nonlinear relationship between the rotor induced acoustic and vibration levels, and second, to generate optimal HHC or IBC pitch control inputs that simultaneously reduce noise and vibration.

As a background to the present neural control study on rotor noise and hub loads, a few relevant studies on the phenomenon of blade vortex interaction (BVI) rotor noise are summarized here. Schmitz (Ref. 1) presents an authoritative discussion on rotor noise including BVI noise, and the research studies by Kitaplioglu, et al. (Ref. 2) and McCluer, et al. (Ref. 3) represent recent research.

With regard to active control inputs, rotorcraft advancing side blade vortex interaction noise (Jacklin, et al., Ref. 4 and Swanson et al., Refs. 5 and 6) and vibratory hub loads (Kottapalli, et al., Ref. 7) almost always behave nonlinearly with respect to the phase of an HHC or IBC input.

In this study, the neural controller is required to be relatively quick in its execution and not be computationally intensive. Thus, the present control procedure is bound by the following ground rules: the controller must converge in six iterations or fewer and gradient-based optimization techniques must not be used. The present study is an extension of an earlier investigation on neural network identification and control of rotorcraft hub loads (Ref. 8). The objective is to develop a robust, neural network based controller to simultaneously minimize advancing side BVI noise and vibratory hub loads (Ref. 9). The noise and hub loads data were obtained from a wind tunnel test of a four-bladed rotor with individual blade control during simulated descent (Ref. 5). These data were obtained from the second U.S./German Individual Blade Control wind tunnel test (Jacklin, et al., Ref. 4, and Swanson et al., Refs. 5 and 6). The test article was a four-bladed BO-105 hingeless rotor system fitted with IBC electro-hydraulic actuators and the test was performed in the NASA Ames 40- by 80-Foot Wind Tunnel. The test condition considered in the present study is an intense-BVI condition ("high-BVI" condition): 65 knots ($\mu = 0.15$), Mtip = 0.64, $\alpha_s = 2.9$ deg, and $C_T/\sigma = 0.075$ (Ref. 5).

Plant Model

Single-Input, Single-Output Plant Model. In the SISO application, the network training input is the 2P control phase input Φ_2 where the pitch control amplitude A_2 is maintained at 1.0 deg. The IBC pitch input is defined as follows:

$$\theta_{im} = A_m \sin [m (\psi_i + 90 \text{ deg}) + \Phi_m] \qquad (1)$$

The network output is the advancing side noise metric (ASNM). Figure 1 (Ref. 5) shows a general layout of the rotor and microphones in the wind tunnel test section. The present ASNM was obtained with the traverse location fixed at the advancing side position X = 16.41 ft. The four sound pressure levels (SPL's) from the four microphones were individually summed over the 6th through 40th blade passage frequency band and subsequently averaged together to give the present band-limited, sound pressure level based ASNM (BL-SPL ASNM).

Accurate plant modeling in the present SISO application was obtained by using a two-hidden-layer radial basis function (RBF) type of neural network (Fig. 3). References 10 and 11 contain more information on how appropriate two-hidden-layered RBF networks are selected as plant models.

Single-Input, Multiple-Output Plant Model. The majority of the present neural network results involve the use of the SIMO plant model. In the SIMO application, the network training input is again the 2P control phase input Φ_2 with $A_2 = 1.0$ deg. The two network outputs are the advancing side noise metric ASNM and the vibratory hub loads metric

VHLM (Fig. 4). Accurate plant modeling was obtained by using a SIMO RBF network.

Objective Function

The present study characterizes the advancing side rotor BVI noise and vibratory hub loads by an objective function. The objective function consists of a weighted sum of the squares of a four-microphone-average of advancing side BVI noise and the vibratory hub loads metric:

$$J = (W_{ASNM}) \, ASNM^2 + VHLM^2 \qquad (2)$$

where W_{ASNM} is a specified weight. For brevity, the advancing side noise and vibratory hub loads objective function is referred to as the noise and hub loads objective function (Ref. 9).

In the present application, W_{ASNM} was selected as 100 (Ref. 9). The introduction of the noise and hub loads objective function J makes the neural network control procedure developed in Ref. 8 directly applicable to the present noise and hub loads control problem (Fig. 2).

Results

Results are presented to assess the neural controller's convergence behavior, robustness, and accuracy. The performance of the neural controller is also compared with a traditional, one-step deterministic controller (Johnson, Ref. 12) as "re-applied" to the first three cases.

Hub Loads Control

The basic variation of VHLM is shown in Fig. 4. The baseline VHLM value is 578. Two clearly defined minimums exist. The IBC test-based global minimum VHLM is 211 (at $\Phi_2 = 240$ deg).

For the hub loads baseline (benchmark) case, Fig. 5 shows a representative output of the present inverted neural network for control (INNC). The present INNC utilizes a simple back-propagation neural network to "locate" the appropriate (global) minimum. Figures 6a and 6b show the convergence of the closed loop hub loads neural network controller to the global minimum.

Figures 7a and 7b show the results for a starting point sensitivity study in which the controller starting points were varied. Four different starting values of the 2P control phase input (0, 180, 240, and 270 deg) is studied. It can be seen from Figs. 7a and 7b that the neural controller is robust in finding a global optimum irrespective of the initial starting point.

Figures 8, 9a and 9b show results related to a reduced data base case in which the number of neural network training points was six compared to the baseline value of 13. Here, the basic noise and hub loads case 12-point data set is split into two smaller 6-point data sets based on odd- and even-numbered selections. This case is important since the results can be used to assess the impact of reducing the number of training data points made available to that part of the neural control procedure which provides an updated estimate of the 2P control phase input. Again, convergence to a global minimum is obtained.

Finally, Figs. 10, 11, 12a, and 12b show neural network control results for the hub loads amplitude-variation case in which a single minimum exists. Figure 10 shows the vibratory hub loads metric variation with 2P control amplitude input A_2 for a constant 2P control phase input $\Phi_2 = 210$ deg. The IBC test-based minimum metric is 328 (at $A_2 = 0.5$ deg). Figure 11 shows the shows the output of the inverted neural network for control for the amplitude-variation case. The neural controller converged to a metric of 346 (Fig. 12a). The corresponding predicted 2P control amplitude is 0.57 deg (Fig. 12b). Comparing this result with Fig. 10, the neural controller has acceptably converged to a minimum VHLM.

Noise and Hub Loads Control

Plant Model. This case addresses simultaneous control of advancing side BVI noise and vibratory hub loads. This case considers the variation of the noise and hub loads objective function with 2P control phase input Φ_2 with a constant control amplitude $A_2 = 1$ deg. The IBC data base for this case has 12 data points ($\Phi_2 = 0$ to 330 deg at 30 deg intervals). For this case, the variation of the advancing side noise metric (ASNM) has an ill-defined minimum (Fig. 3). At the same time, for this relatively flat minimum, Φ_2 values between 150 deg and 240 deg are acceptable control inputs that will result in acceptably low advancing side noise levels. The vibratory hub loads metric input data was shown in Fig. 4. The neural control procedure is initiated with a 2P control phase input $\Phi_{2N,\,0} = 0$ deg. Figure 13 shows the advancing side noise

metric and the vibratory hub loads metric on a plot with two vertical axes. In the figure, the solid circles represent the measured advancing side noise metric values and the solid squares represent the measured vibratory hub loads metric values. The baseline (no IBC, $A_2 = 0$ deg) ASNM value is 116 dB. The IBC test-based minimum ASNM is 108 dB (at $\Phi_2 = 210$ deg). Figure 13 also shows the plant modeling results obtained from the SIMO RBF neural network. This SIMO RBF neural network is also used as the plant model in the basic noise and hub loads control case and the starting point sensitivity case.

The IBC test-based baseline value (no IBC input, $A_2 = 0$ deg) of the above combined noise and hub loads objective function ($W_{ASNM} = 100$) was 1.68×10^6 (Fig. 14); with an IBC input of $A_2 = 1$ deg, the minimum value of this objective function occurred at $\Phi_2 = 240$ deg and J was 1.23×10^6.

Figure 14 shows that the present noise and hub loads objective function J does not appear to have a minimum as well-defined as the minimum in the VHLM variation (Fig. 13). The VHLM variation (Figs. 4 and 13) has two clearly defined minimums, whereas Fig. 14 shows that a relatively flat minimum exists for the present objective function.

Neural Controller Convergence. The neural controller produces a converged minimum noise and hub loads objective function ($J = 1.30 \times 10^6$) in three iterations (Fig. 15a). The corresponding converged optimal 2P control phase input (Φ_{2N}, 3) predicted by the neural controller is 240 deg (Fig. 15b). Figures 16a and 16b show the advancing side noise metric and vibratory hub loads metric corresponding to the 2P control phase input results shown in Fig. 15b.

The neural controller produces a converged minimum advancing side noise metric (111 dB) and a converged minimum vibratory hub loads metric (267). Thus, the neural controller is able to achieve simultaneous reductions of 5 dB in the advancing side noise metric and 54% in the vibratory hub loads metric, with respect to the baseline metrics (Ref. 9).

Starting Point Sensitivity. Four different starting values of the 2P control phase input (0, 180, 240, and 270 deg) is studied. The objective function converged to a value of 1.30×10^6 for all four subcases. The corresponding predicted, converged 2P control phase input is 240 deg for all four subcases.

The converged values are the same as in the basic noise and hub loads case. For this problem, the present noise and hub loads neural controller is insensitive (robust) to starting point.

Reduced Data Base. The plant model for this case is the same as that used in the basic noise and hub loads case. In order to obtain simultaneous reductions in the noise and hub loads in the reduced data base cases, a nonlinear transformation (scaling) of the objective function was introduced (Ref. 9). For the *odd-numbered, six-point case*, the noise and hub loads neural controller was able to achieve simultaneous reductions of 3 dB (taking into account round-off error) in the advancing side noise metric and 61% in the vibratory hub loads metric. For the *even numbered, six-point case*, the neural controller was able to achieve simultaneous reductions of 6 dB in the advancing side noise metric and 45% in the vibratory hub loads metric.

These noise and hub loads application results indicate that the inverted neural network for control modeling step is sufficiently robust and accurate for the present control purposes involving simultaneous control of noise and hub loads.

One-Step Deterministic Controller. The one-step deterministic controller application used one advancing side noise metric (average) and ten vibratory hub load components (4P sine and cosine components of five hub load components). Separate single harmonic sine and cosine least-square fits from twelve measurements (2P control phase input varying from 0 deg to 330 deg in 30 deg increments) are used to determine the elements of the T-matrix.

The optimal control input is calculated based on a quadratic performance function with the advancing side noise metric weighted 100 times more than the vibratory hub loads components, with all vibratory hub loads responses equally weighted. The performance function is:

$$J = \{ z \}^T [W_Z] \{ z \}$$

For the present one-step deterministic controller, the optimal control input vector is calculated from the procedure given in Ref. 9. The 2×1 vector of optimal control inputs $\{ \theta^* \}$ consists of the sine and cosine components from which the 2P control optimal phase input is calculated. In the following, the subscript "s" refers to the starting condition for the one-step deterministic controller.

Baseline Results: The starting condition is $\{ \theta \}_S = \{ 0 \}$ deg (no IBC, $A_2 = 0$ deg), and with the starting response vector $\{ z \}_S$ taken as the baseline experimental advancing side noise metric and hub loads vector (ten vibratory hub load sine and cosine components). Here, ASNM and VHLM are calculated using the plant model of the basic noise and hub loads case and requiring that the 2P control amplitude input is 1 deg.

The present one-step, noise and hub loads deterministic controller predicts an optimal 2P control phase input of 207 deg. The corresponding advancing side noise metric was calculated to be 107 dB and the vibratory hub loads metric was 507. The present observation is that the two control methods give different minimums. The one-step deterministic controller gives an "acoustic" solution in which only the noise is reduced with a small reduction in the vibration. The neural controller simultaneously controls both acoustic and vibration levels, with substantial reductions in both.

Starting Point Sensitivity: Each of the four sets of $\{ \theta \}_S$ and $\{ z \}_S$ vectors is separately determined by the following four 2P control phase input values: 0, 180, 240, and 270 deg , each with $A_2 = 1$ deg. The control input vector $\{ \theta \}_S$ is directly obtained from the 2P control phase input under consideration, and the starting response vector $\{ z \}_S$ is taken as the experimental advancing side noise metric and the hub loads vector corresponding to the particular 2P control phase input under consideration.

The one-step deterministic controller results are shown in Table 1. Comparison shows that the two control methods can give different solutions, with neural control being more robust. The one-step deterministic controller yields relatively poor simultaneous reductions for the 270 deg starting condition as compared to the corresponding neural network result.

TEST DATA VALIDATION

Introduction

Wind tunnel tests of models provide valuable data. The advantage of rotorcraft wind tunnel testing is that a rotorcraft model can be evaluated for many design variations and rigorously tested prior to its first flight test. The wind tunnel is a facility that can be used

Table 1. Starting Point Sensitivity, One-Step Deterministic Control, A_2=1 deg

Starting 2P control phase phase input deg	Predicted ASNM/ VHLM	Predicted 2P control input deg
0	111 dB / 253	242
180	112 dB / 243	244
240	111 dB / 270	240
270	108 dB / 533	195

over and over again. Thus, wind tunnel testing is less expensive and safer than flight testing.

Wind tunnel testing often uses a matrix testing approach. In this type of testing, there are significant variations in the test conditions, which can be well outside flight conditions. A wind tunnel test can also encompass a larger "test envelope" compared to a flight test because of safety considerations which preclude testing in flight. As such, it is difficult at times to even heuristically know the measured data functionality as it varies with the test condition. Therefore, it is difficult to quickly isolate any bad data points or, even more difficult, to interpret the quality of the measured data (Kottapalli, Ref. 13). Thus, validating rotary wing wind tunnel test data is important to a successful test. It is anticipated that for purposes of wind tunnel testing, a successful neural network application may enable "near on line" data quality checks and subsequent post-run assessment of data goodness.

Also, for outdoor hover testing, the influence of winds has to be properly accounted for when correcting and analyzing the outdoor test data. Thus, there is a second need for consistent, easy-to-understand and easy-to-apply wind corrections to outdoor hover performance test data. The present study also includes the use of neural networks to obtain physical insight related to outdoor hover wind corrections (Ref. 13).

In the present context, the use of neural networks is justified because of their multi-dimensional, nonlinear curve fitting characteristics. The present work is considered to be a generic methodology. The present neural network data validation representations and quality assessments, and the neural-network-based procedure for wind corrections, are not specific to the presently-considered tilt-rotor configuration, i.e., they

can be applied to rotor testing in general, with extension to fixed wing testing as well.

Tilt-Rotor Test Data Base

Wind Tunnel Hover and Forward Flight Test Data.
Full-scale XV-15 tilt rotor test data covering both hover and forward flight conditions were acquired by Light (Ref. 14). The XV-15 tilt-rotor right hand rotor only (25 ft diameter) was installed on the NASA Ames Rotor Test Apparatus and tested in the NASA Ames 80- by 120-Foot Wind Tunnel. In hover, the shaft angle was varied from -15 deg to +15 deg. For purposes of the present neural network study, the XV-15 tilt-rotor hover 80- by 120-Foot Wind Tunnel test data base consisted of approximately 90 data points. The relevant rotor performance variables in hover were the rotor torque coefficient (C_Q) and the figure of merit (FM).

In forward flight, the lateral and longitudinal cyclic pitch, pitch link loads, and the blade yoke chordwise and flatwise bending moments are included. The forward flight test data base consisted of approximately 275 data points. These data were acquired at wind tunnel speeds up to 80 knots.

Outdoor Hover Test Data. The full-scale outdoor XV-15 tilt-rotor hover test data base was acquired by Felker, et al. (Refs. 15, 16). The same XV-15 tilt-rotor right hand only was installed on the NASA Ames Propeller Test Rig and tested at the outdoor facility. Both axial and lateral wind measurements were taken, thus bringing in two additional variables into this problem. For purposes of the present neural network study, the outdoor XV-15 tilt-rotor hover test data base (Ref. 15) consisted of approximately 150 data points and included those data points taken with winds up to speeds of 3.5 m/s (referred to as the "all winds" data base). The relevant rotor hover performance variables were C_Q and FM. The present neural network study considers hover test data with a rotor hover tip Mach number (M_{tip}) of 0.69 only.

Results - Wind Tunnel

Wind Tunnel, Hover

Measured and Derived Neural Network Inputs. Two back-propagation networks were trained with two different sets of inputs and outputs. The two cases were identified by the following descriptors: "measured" inputs and "derived" inputs. "Measured" input variables refer to directly measured variables, and are, for example, discrete sensors. "Derived"

input variables refer to variables that perhaps make more sense physically and, for example, are obtained from rotor balance measurements, resulting in a final, reliable thrust or torque level. Table 2 below shows the associated neural network inputs and outputs.

Table 2. Neural Network Inputs and Outputs

Case	Inputs	Outputs
Measured	Θ_0, α_s	$C_T/\sigma, C_Q$, FM
Derived	$C_T/\sigma, \alpha_s$	Θ_0, C_Q, FM

Figures 17 and 18 show the results from two MIMO back-propagation networks with inputs and outputs as shown above. For the measured inputs case (Fig. 17), the correlation plot shows that the predicted C_T/σ versus test C_T/σ variation falls off at the highest thrust levels. For the derived inputs case (Fig. 18), the correlation plot shows that the predicted Θ_0 versus test Θ_0 variation is close to a straight line at 45 deg. The back-propagation network with the derived parameters as network inputs was judged to represent the available test data more accurately. Therefore, this study uses C_T/σ as a neural network input parameter for all neural networks developed in this study. This is in part due to the high accuracy of the balance used in the Rotor Test Apparatus to measure C_T/σ.

Figure of Merit versus C_T/σ Variation. Figure 19 shows the results of three simple SISO back-propagation neural network fits, where the network input was C_T/σ and the network output was the figure of merit. Each neural network is for a fixed shaft angle. Note the drop-off in the test figure of merit at very high values of the thrust. This is basically due to rotor blade stall, a limiting condition. The neural-network-based figure of merit representations of Fig. 19 did not extrapolate rotor stall for this wind tunnel data base.

Figure 20 shows the result of a single MIMO back-propagation neural network fit, where the network inputs were $C_T/\sigma, \alpha_s$ and the network outputs were Θ_0, C_Q, and FM. Both global and "subtle" effects are captured by this relatively complex MIMO back-propagation neural network. The sensitivity of the figure of merit to the shaft angle is captured for the range of test thrust levels. However, similar to the

above SISO application, the neural-network-based figure of merit representations did not extrapolate rotor stall for this wind tunnel data base. The advantage of the MIMO representation is that all test conditions can be included as inputs to a single neural network without sacrificing accuracy, yet are valid only within the range of the training data. Also, unlike the SISO neural network extrapolations which are not level and actually show a continuing increase in the figure of merit with further increases in C_T/σ, the MIMO neural network representations provide almost-level extrapolations.

Wind Tunnel, Forward Flight

The following wind tunnel test parameters were selected as the forward flight neural network inputs: α_s, μ, and C_T/σ. The neural network outputs for individual cases are noted in individual case-descriptions as follows.

Wind Tunnel Controls. The measured collective variation (Ref. 14) with the shaft angle for the test data acquired is shown in Fig. 21. Reference 13 contains the results for the two cyclic pitch controls. Figure 22 shows the present correlation plot from a MIMO back-propagation neural network, where the neural network outputs were the collective, lateral and longitudinal cyclics. The present neural-network-based representations for the wind tunnel test controls are considered to be very good. Thus, the quality of the controls test data is acceptable. The use of the collective pitch as a neural network output is valid even though its use as a neural network input is not valid. Thus, neural networks can be used for compact representation of test data control inputs, along with other variables of interest considered in the following discussions.

Oscillatory Pitch Link Loads. The forward flight oscillatory test pitch link load variation (Ref. 14) with shaft angle is shown in Fig. 23. Figure 24 shows the correlation plot from a MISO back-propagation neural network, where the neural network output was the oscillatory pitch link load. The present neural-network-based representation for the oscillatory pitch link loads is within 10 lb of the correlation line, Fig. 24. This oscillatory-pitch-link-loads correlation was considered to be very good. This is due to the fact that during a forward flight test condition, the rotor blade pitch links are subjected to high dynamic loading which is often due to nonlinear aerodynamic blade loading. Thus, the pitch link loads data base would have a wider "uncertainty band" due to the pitch links operating in an environment that is dynamic. In any case, the quality of the present pitch link load test data is acceptable.

Blade Flatwise Bending Moments. Figures 25 and 26 show the correlation plots from a MIMO back-propagation neural network, where the neural network outputs were the mean and oscillatory flatwise bending moments. For the mean and oscillatory flatwise bending moments, points far away from the correlation line are associated with bad test data points. It was found that some data points were not repeatable, possibly due to instrumentation problems. Indeed, the present neural network analysis raises questions about the useability of approximately 5% of the flatwise bending moment database. This is an example of the ability of neural networks to capture poor data quality.

Blade Chordwise Bending Moments. The forward flight test blade yoke chordwise mean and oscillatory bending moments were considered in the present neural network study. Figures 27 and 28 show the present correlation plots from a MIMO back-propagation neural network, where the neural network outputs were the mean and oscillatory chordwise bending moments. The neural-network-based representations were very good for the blade yoke mean and oscillatory chordwise bending moments. The present neural network analysis shows that the chordwise bending moment data are useable and are of good quality as a whole.

Results - Outdoor, Hover Wind Corrections

Existing, Momentum-Theory-Based Wind Correction Method. Felker, et al. (Refs. 15, 16) present a wind correction procedure based on momentum theory. The procedure was developed by W. Johnson of NASA Ames and M. A. McVeigh of Boeing Defense Systems (Helicopters). The existing, momentum-theory-based wind corrected rotor torque coefficient C_{QCORRM} was obtained from the equations given in Refs. 15 and 16. The corrected figure of merit data from Ref. 15 were used in the present neural network study only for comparison purposes. The uncorrected outdoor test data points (Ref. 15) are shown in Fig. 29.

Neural-Network-Based Wind Correction Procedure. The present neural network wind correction procedure deals only with outdoor hover test data. This procedure makes use of a "zero wind" neural network representation. The zero wind neural network representations are reference variations that represent isolated rotor tilt-rotor hover performance, and which

by definition do not require any wind corrections. In the present study, the performance variables were as follows: C_Q and FM, and for the zero wind case depend only on C_T/σ. In the present study, test data points with wind speeds < 0.5 m/s were defined to be zero wind points. The zero wind figure of merit representation, referred to as FM_{ZW}, is a function of only C_T/σ. A SIMO two-hidden-layer back-propagation network with one input, C_T/σ and three outputs Θ_0, C_Q, and FM was used in the present study to obtain FM_{ZW}.

A MISO two-hidden-layer back-propagation network with three inputs C_T/σ, μ_x, and μ_y, and one output Δ_T was trained in order to predict the FM-deltas. The neural-network-predicted FM-deltas are referred to as $\Delta_{TNN}(C_T/\sigma, \mu_x, \mu_y)$ and represent the necessary wind corrections to yield the isolated rotor zero wind hover performance. Details are given in Ref. 13.

Neural-Network-Based Wind Corrections The present zero wind neural network representation was derived using 25 test data points. Figure 30 shows these data points and the resulting neural network representation derived from the SIMO back-propagation neural network. Figure 31 shows both the test-based and the MISO neural-network-predicted FM-deltas.

Figure 32 shows the corrected figure of merit obtained from the present neural network approach and also, as the reference curve, the zero wind neural network representation, Fig. 30. Figure 32 shows that the present neural-network-based wind correction procedure gives very satisfactory corrections. Figure 33 shows Felker's corrected figure of merit (Ref. 15) The present neural-network-based figure of merit corrections are more accurate than Felker's corrections. The RMS errors associated with the present neural-network-corrected figure of merit (0.01) and Felker's corrected figure of merit (0.02) quantitatively demonstrate that the present neural-network-based wind corrections are more accurate compared to the existing wind corrections.

Physical Interpretations from Neural Networks. Compared to the existing, momentum-theory-based wind corrections model, the present neural-network-based procedure for wind corrections can represent the actual (e.g., physical) trends present in the test data, and thus be able to provide insight into the required wind corrections. These physical trends could be linear or nonlinear, "subtle" or "gross." The momentum-theory-based wind corrections would not be able to capture those trends that fall outside of the momentum theory's domain of applicability.

The above mentioned physics-related advantage of neural networks was studied using a simple example as follows. As a typical operating condition, consider $C_T/\sigma \approx 0.12$. In this example, the figure of merit deltas (FM-deltas or wind corrections) for zero lateral wind condition with varying axial velocity and separately, for zero axial wind condition with varying lateral velocity, were considered. One set of FM-deltas was obtained using the previously-trained MISO back-propagation neural network (this neural network was trained using the complete outdoor test data base). The second set of FM-deltas was obtained using the existing, momentum-theory-based equations (Ref. 16). Figures 34 and 35 show the resulting FM-deltas for this example.

Figure 34 shows that both the nonlinear, neural-network-based and almost-linear, momentum-theory-based representations are basically the same for the effect of the axial wind (with zero lateral wind).

Figure 35 shows the effect of the lateral wind (with zero axial wind) on the FM-deltas. The neural-network-based and the momentum-theory-based representations are different. The neural-network-based FM-deltas have a value of -0.02 (for negative lateral winds) and it was separately verified that this "trend" does represent the test data. The existing, momentum-theory-based FM-deltas, also shown in Fig. 35, have a magnitude much smaller than 0.02. Thus, the existing, momentum-theory-wind-correction formulation "misses" some physical trends present in the test data. A possible explanation is as follows. The momentum-theory-based wind correction (Ref. 16) for non-negligible lateral wind (with zero axial wind) is dependent on the product of the lateral wind and the very small in-plane force C_Y, resulting in a momentum-theory-based wind correction that is negligible. This is contrary to the trend present in the outdoor hover test data base under consideration. Thus, the neural network is able to capture the physical trends that are present in full-scale test data and give a more realistic representation.

CONCLUDING REMARKS

Identification and Control

The application of neural networks to rotorcraft dynamics and acoustics control is still relatively new. The objective of the present noise and hub loads study was to develop a robust neural-network-based

controller to simultaneously minimize BVI noise and vibratory hub loads. An objective function consisting of the weighted sum of advancing-side-BVI-noise and a vibratory-hub-loads-metric was used to characterize the rotor BVI noise and vibratory hub loads.

The noise and hub loads neural network controller was successful in achieving convergence within a limited number of iterations while being robust and computationally efficient. Specific findings from the present identification and control study were as follows:

1. The present neural network controller successfully achieved the objective of simultaneous, substantial reductions in advancing side blade vortex interaction noise (5 dB reduction) and in vibratory hub loads (54% reduction) within six iterations without using gradient-based optimization techniques.

2. The results showed that the present neural control procedure is robust.

3. A comparison of the results from the present noise and hub loads neural controller with those from a one-step deterministic controller showed that the two control methods can give different solutions, with neural control being more robust.

Test Data Validation

Specific findings from the present full-scale rotor test data validation study were as follows:

1. Neural networks were successfully used to represent and assess the quality of tilt-rotor hover and forward flight performance test data. Neural networks accurately captured tilt-rotor performance at steady operating conditions.

2. In forward flight, the wind tunnel test data were generally of very high quality. Approximately 5% of the existing data base for the blade flatwise bending moments at the yoke were shown to be of poor quality using neural networks.

3. Compared to existing, momentum-theory-method based wind corrections to outdoor hover performance, the present neural-network-procedure-based corrections were better.

4. The present wind corrections procedure, based on well-trained neural networks, captured physical trends present in the outdoor hover test data that had been missed by the existing, momentum-theory-based method.

REFERENCES

1. Schmitz, F.H., "Rotor Noise," Aeroacoustics of Flight Vehicles: Theory and Practice, Volume 1: Noise Sources, NASA Reference Publication 1258, Vol. 1, WRDC Technical Report 90-3052, 1991.

2. Kitaplioglu , C., Caradonna, F.X., and Burley, C.L., "Parallel Blade-Vortex Interactions: An Experimental Study and Comparison with Computations," American Helicopter Society Second International Aeromechanics Specialists Conference, Bridgeport, Connecticut, October 1995.

3. McCluer, M., Baeder, J.D., and Kitaplioglu, C., "Comparison of Experimental and Blade-Vortex Interaction Noise with Computational Fluid Dynamic Calculations," American Helicopter Society 51st Annual Forum, Fort Worth, Texas, May 1995.

4. Jacklin, S., Blaas, A., Kube, R., and Teves, D., "Reduction of Helicopter BVI Noise, Vibration, and Power Consumption through Individual Blade Control," American Helicopter Society 51st Annual Forum, Ft. Worth, Texas, May 1995.

5. Swanson, S., Jacklin, S.A., Blaas, A., Niesl, G., and Kube, R., "Acoustic Results from a Full-Scale Wind Tunnel Test Evaluating Individual Blade Control," American Helicopter Society 51st Annual Forum, Fort Worth, Texas, May 1995.

6. Swanson, S., Jacklin, S.A., Blaas, A., Kube, R., and Niesl, G., "Individual Blade Control Effects on Blade-Vortex Interaction Noise," American Helicopter Society 50th Annual Forum, Washington, D.C., May 1994.

7. Kottapalli, S., Swanson, S., LeMasurier, P., and Wang, J., "Full-Scale Higher Harmonic Control Research to Reduce Hub Loads and Noise," American Helicopter Society 49th Annual Forum, St. Louis, Missouri, May 1993.

8. Kottapalli, S., "Identification and Control of Rotorcraft Hub Loads Using Neural Networks," American Helicopter Society 53rd Annual Forum, Virginia Beach, Virginia, April 1997.

9. Kottapalli, S., "Exploratory Study on Neural Control of Rotor Noise and Hub Loads," American Helicopter Society Technical Specialists' Meeting for Rotorcraft Acoustics and Aerodynamics, Williamsburg, Virginia, October 1997.

10. Kottapalli, S., Abrego, A., and Jacklin, S., "Application of Neural Networks to Model and Predict Rotorcraft Hub Loads," American Helicopter Society Second International Aeromechanics Specialists Conference, Bridgeport, Connecticut, October 1995.

11. Kottapalli, S., Abrego, A., and Jacklin, S., "Multiple-Input, Multiple-Output Application of Neural Networks to Model and Predict Rotorcraft Hub Loads," Sixth International Workshop on Dynamics and Aeroelastic Stability of Rotorcraft Systems, Los Angeles, California, November 1995.

12. Johnson, W., "Self-Tuning Regulators for Multicyclic Control of Helicopter Vibration," NASA Technical Paper 1996, March 1982.

13. Kottapalli, S., "Neural Network Research on Validating Experimental Tilt-Rotor Performance," AIAA-98-2418, 16th AIAA Applied Aerodynamics Conference, Albuquerque, New Mexico, June 1998,

14. Light, J., "Results from an XV-15 Rotor Test in the National Full-Scale Aerodynamics Complex," American Helicopter Society 53rd Annual Forum, Virginia Beach, Virginia, April 1997.

15. Felker, F.F., Betzina, M.D., and Signor, D.B., "Performance and Loads Data from a Hover Test of a Full-Scale XV-15 Rotor," NASA Technical Memorandum 86833, November 1985.

16. Felker, F.F., Maisel, M.D., and Betzina, M.D., "Full-Scale Tilt-Rotor Hover Performance," *Journal of the American Helicopter Society*, April 1986, pp. 10-18.
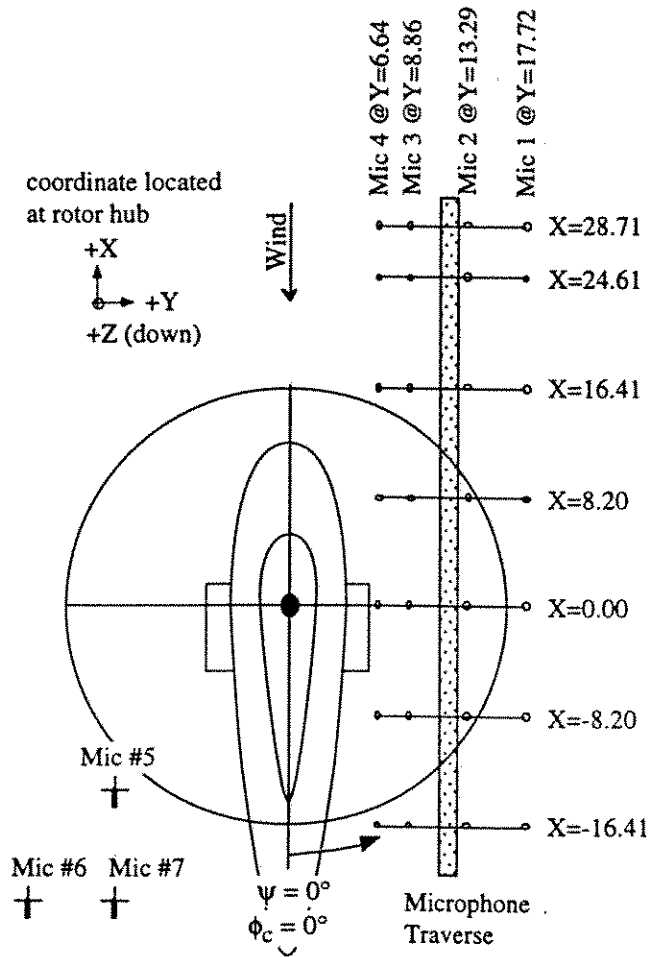
Fig. 1 General layout of rotor and microphones in wind tunnel test section (Swanson, et al., Ref. 5)
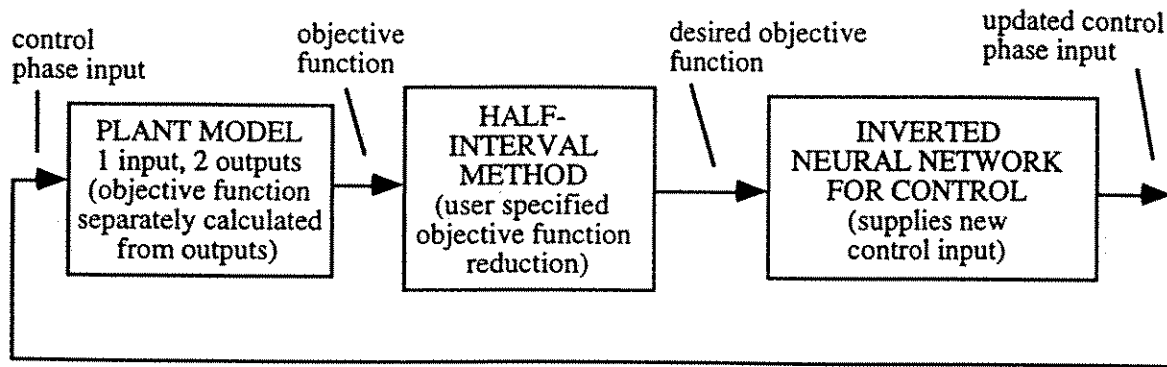
Fig. 2. Overall neural network control procedure for reducing noise and hub loads
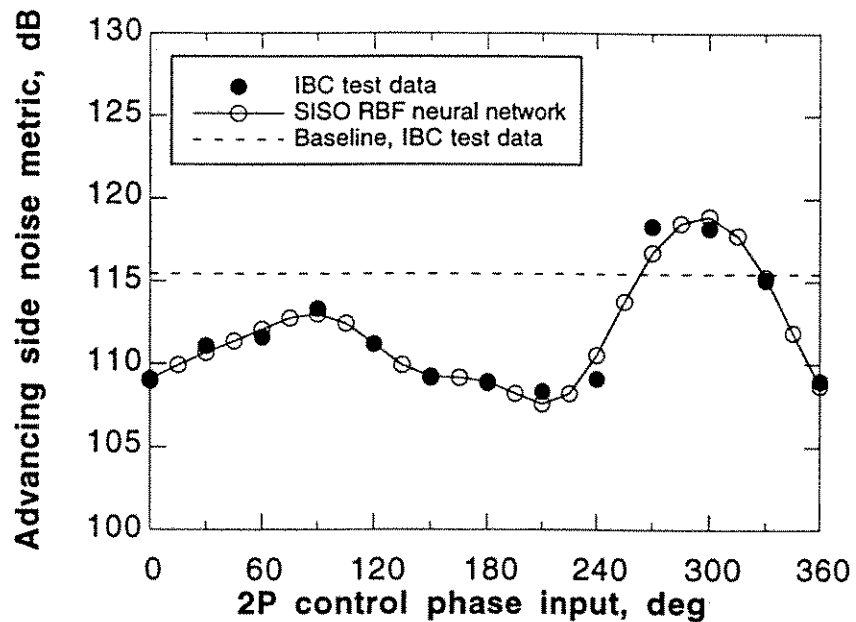
Fig. 3. Experimental noise metric and plant modeling by neural networks
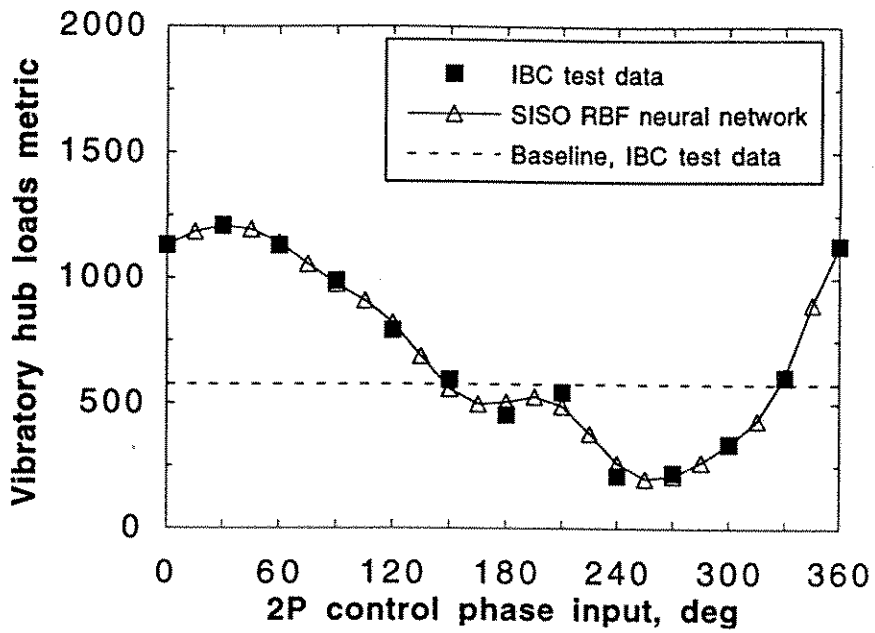
Fig. 4. Hub Loads Control: Experimentally-derived metric and neural-network based identification (plant modeling)
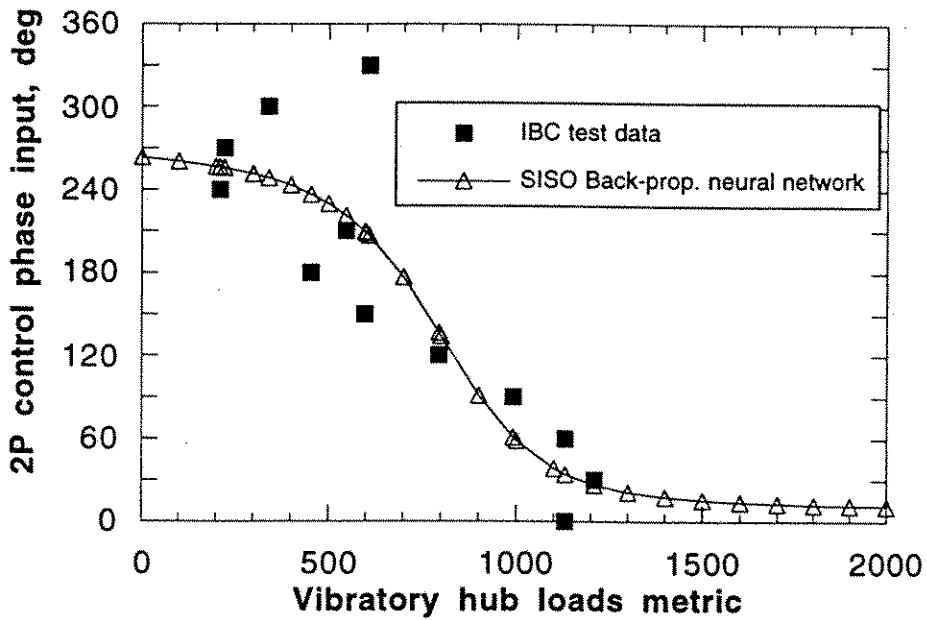
Fig. 5. Hub Loads Control: Basic (Benchmark), output of inverted neural network for control, 12 training points
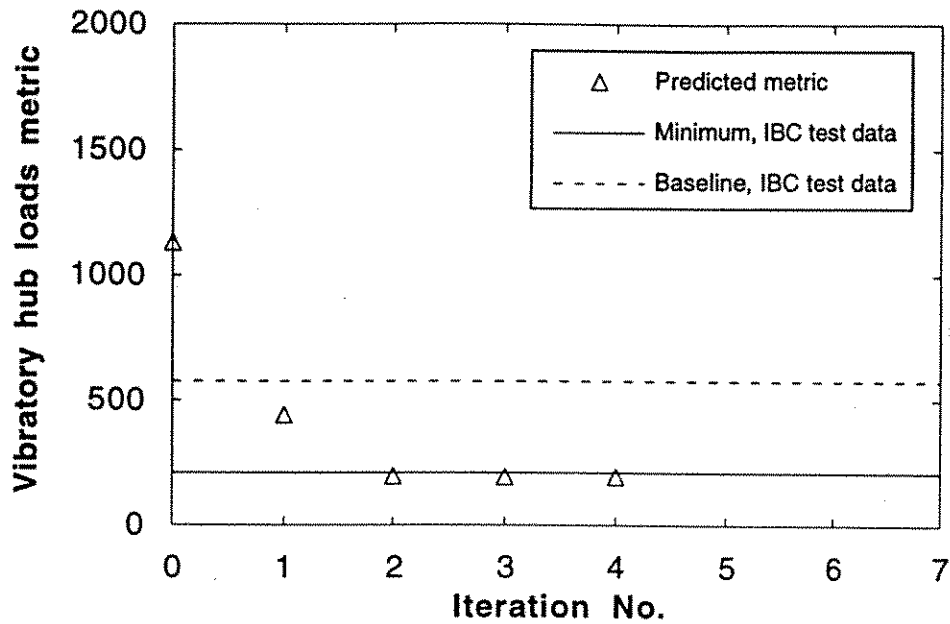
Fig. 6a.   Hub Loads Control: Basic (Benchmark), neural control of hub loads
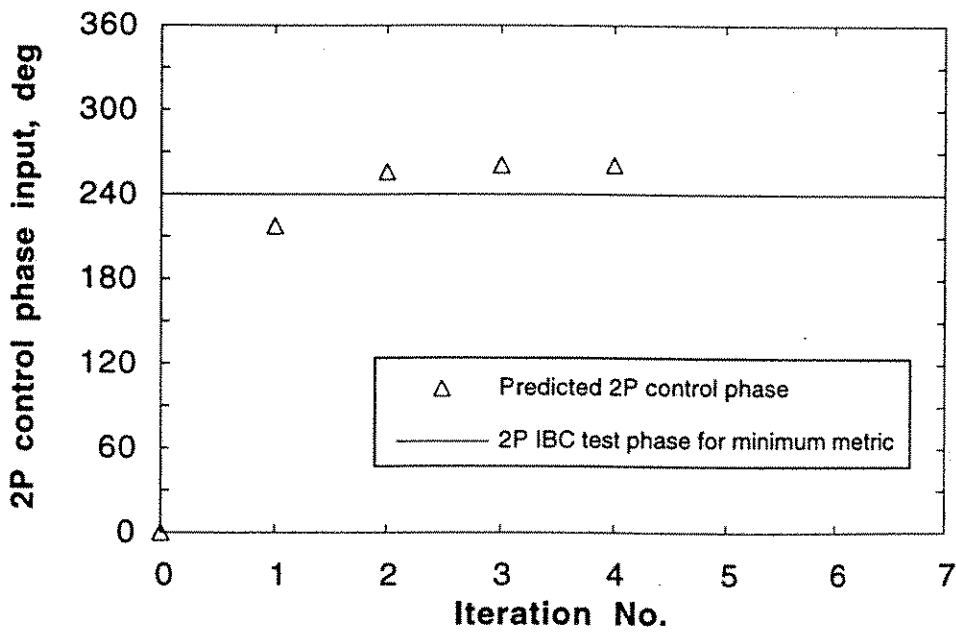
Fig.6b.   Hub Loads Control: Basic (Benchmark), convergence of 2P control phase input (neural control, see Fig. 6a also)
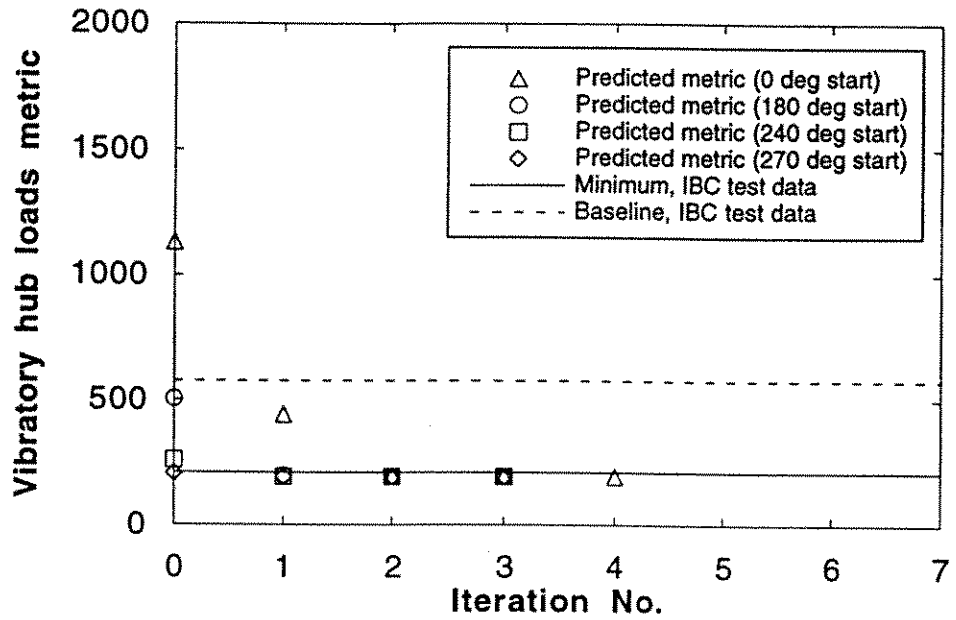
Fig. 7a. Hub Loads Control: Starting Point Sensitivity, convergence of hub loads metric (neural control).
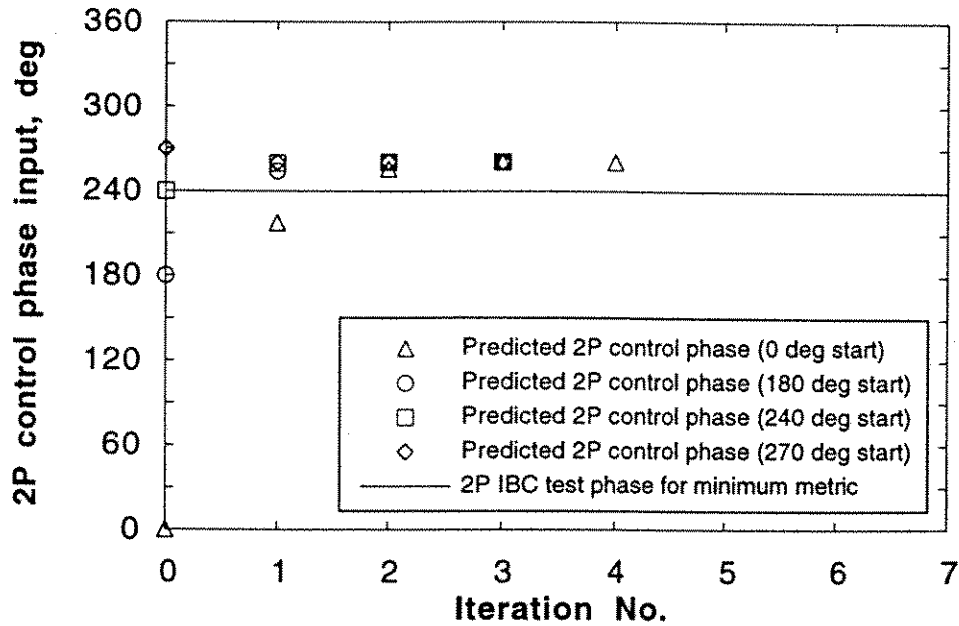
Fig. 7b. Hub Loads Control: Starting Point Sensitivity, convergence of 2P control phase input (neural control, see Fig. 7a also).
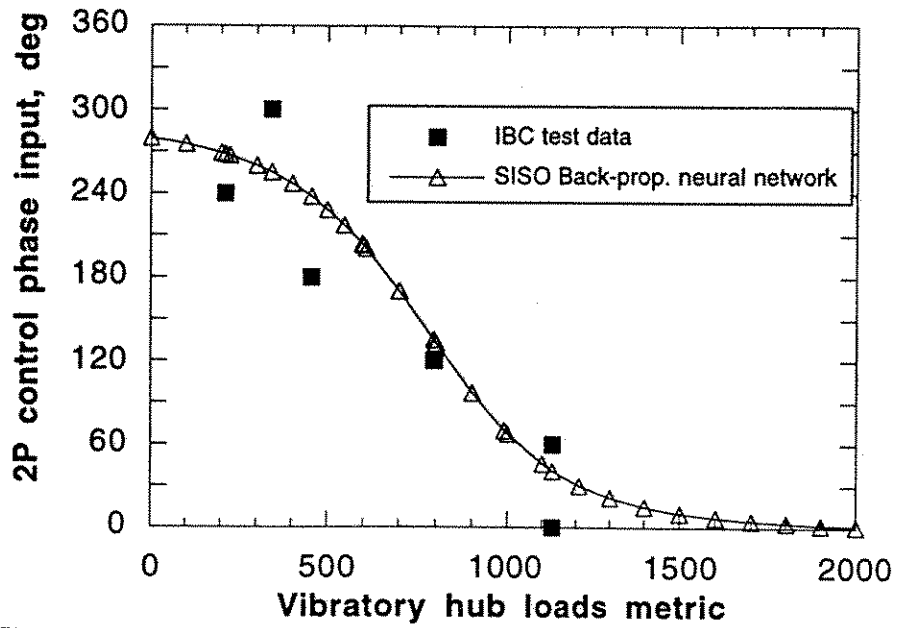
Fig. 8.   Hub Loads Control: Odd-Numbered, Six Point Data Base, output of inverted neural network for control
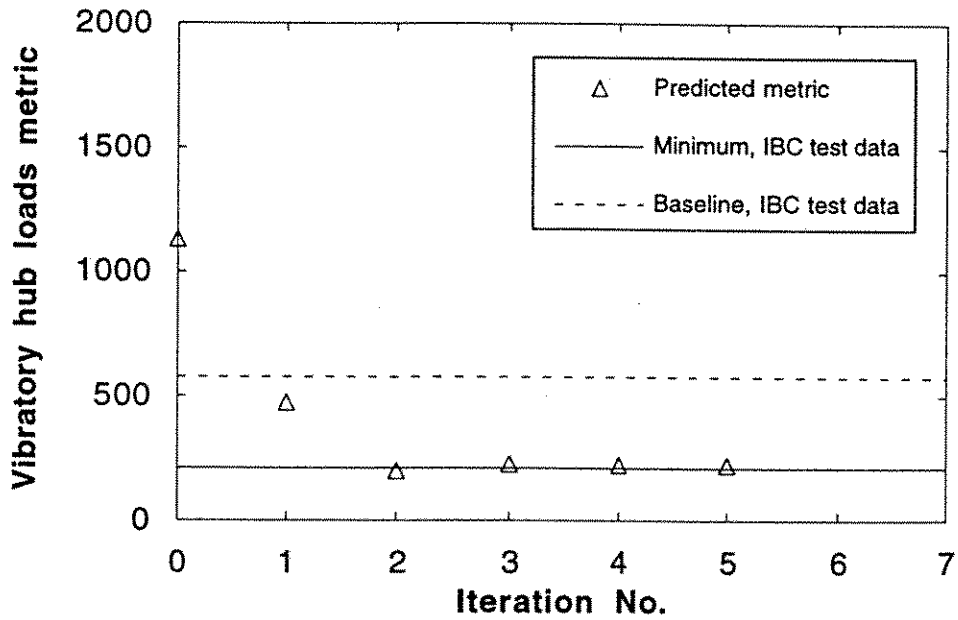
Fig. 9a.   Hub Loads Control: Odd-Numbered, Six Point Data Base, neural control of hub loads metric.
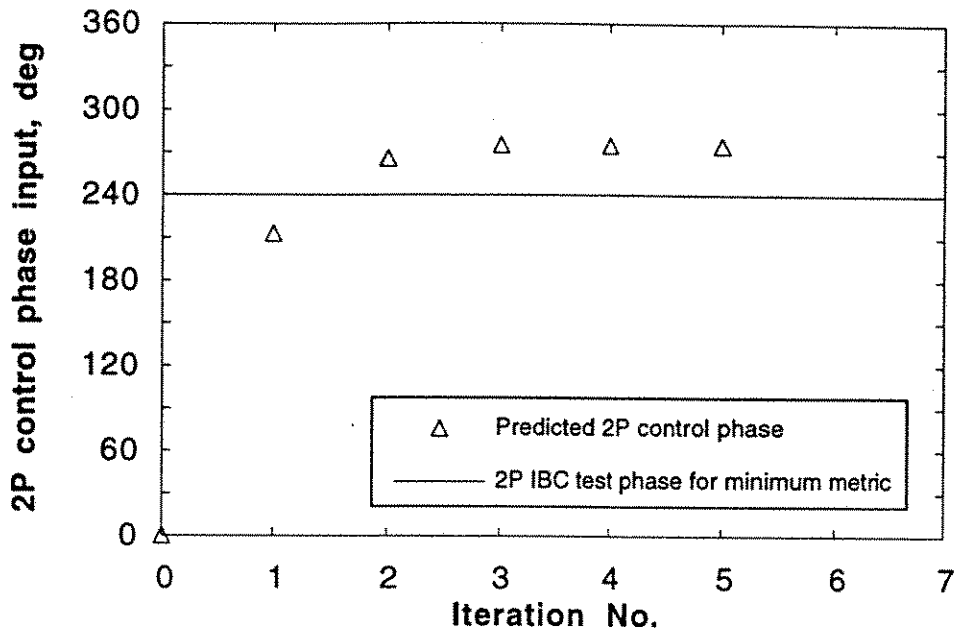
Fig. 9b. Hub Loads Control: Odd-Numbered, Six Point Data Base, convergence of 2P control phase input (neural control, see Fig. 9a also).
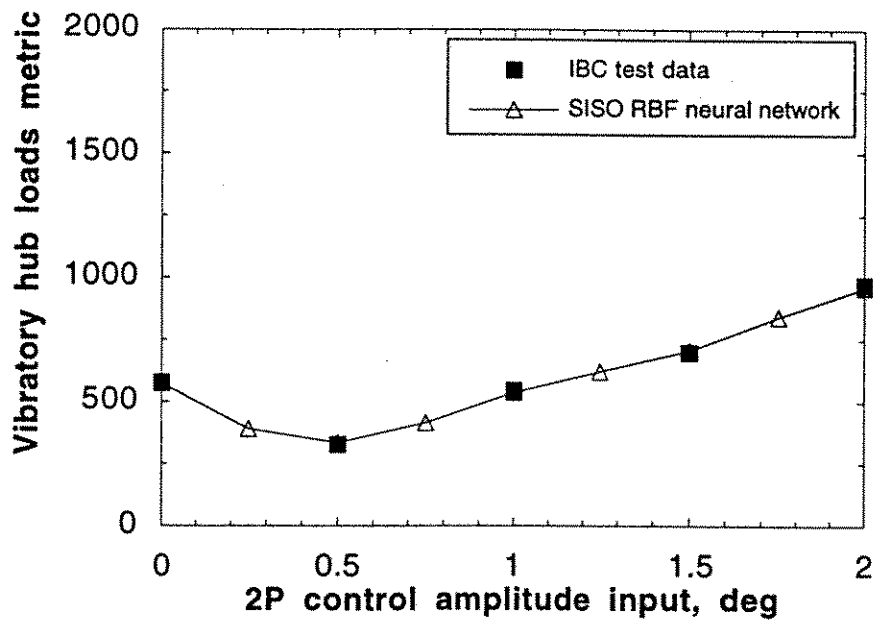
Fig. 10. Hub Loads Control: Experimentally derived metric with amplitude variation, and identification by neural networks (2P control phase=210 deg)
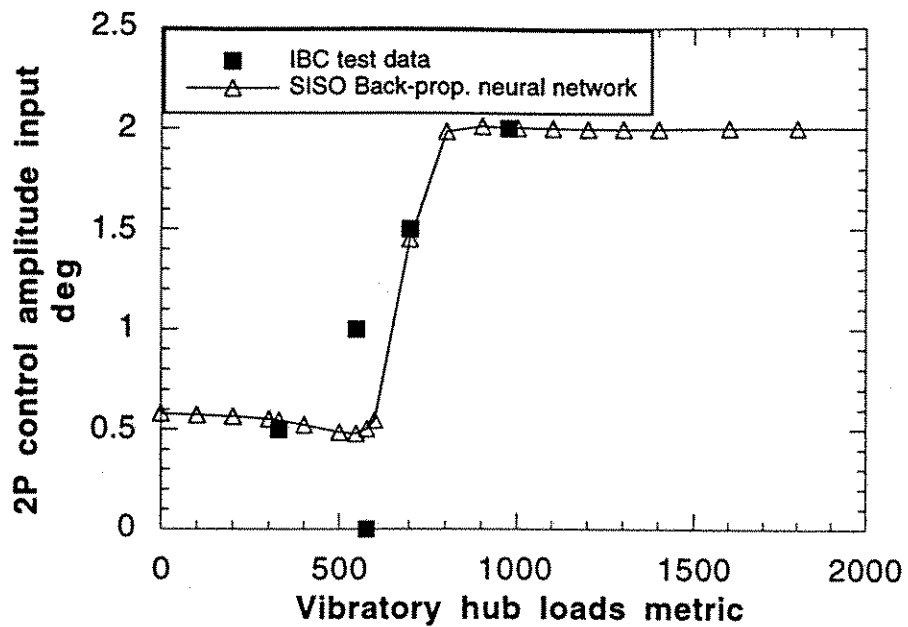
Fig. 11. Hub Loads Control: Amplitude Variation, output of inverted neural network for control, five training points (2P control phase=210 deg)
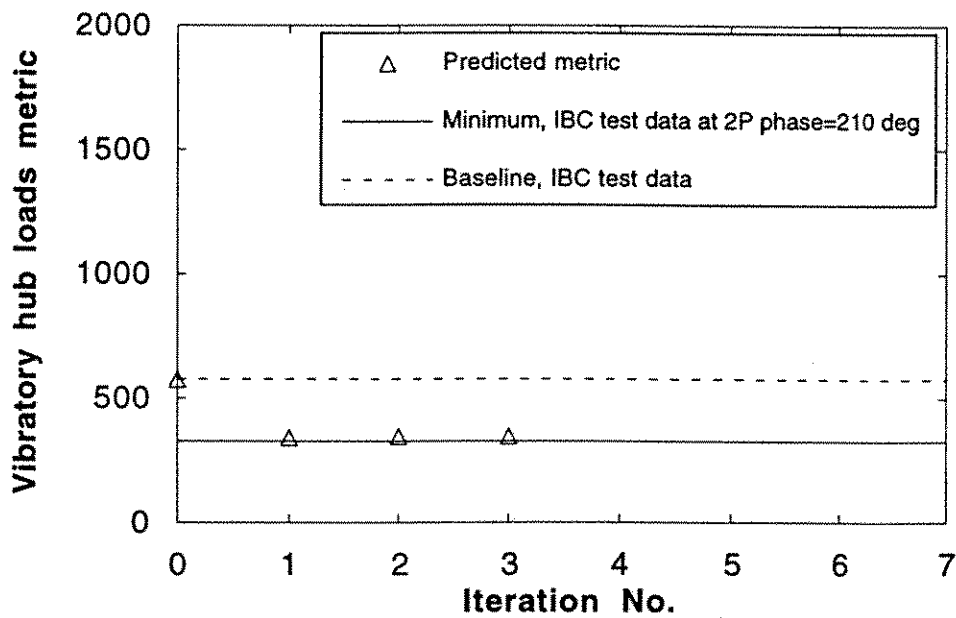
Fig. 12a. Hub Loads Control: Amplitude Variation, neural control
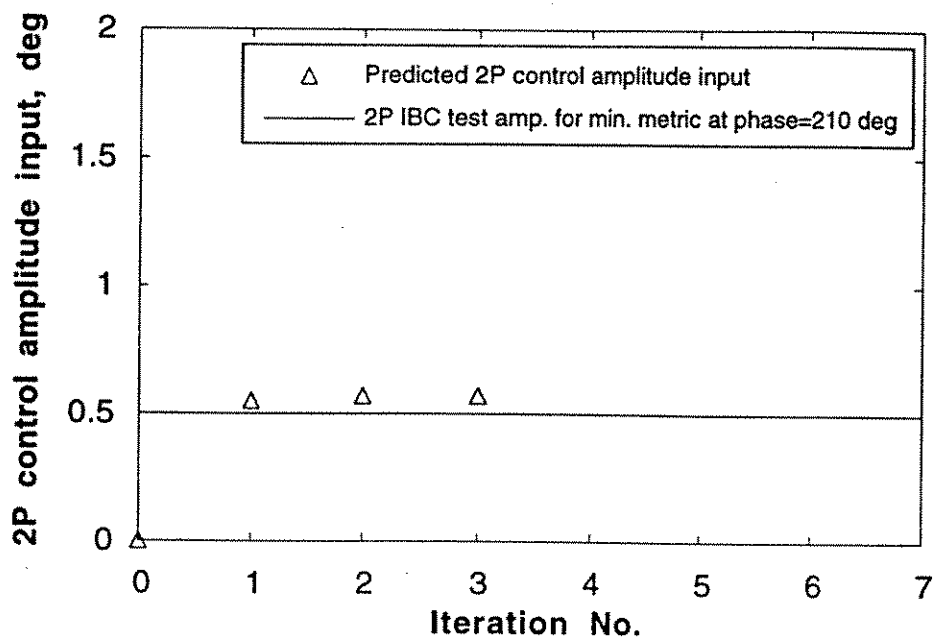
Fig. 12b. Hub Loads Control: Amplitude Variation convergence of 2P control amplitude input (neural control, see Fig. 12a also)
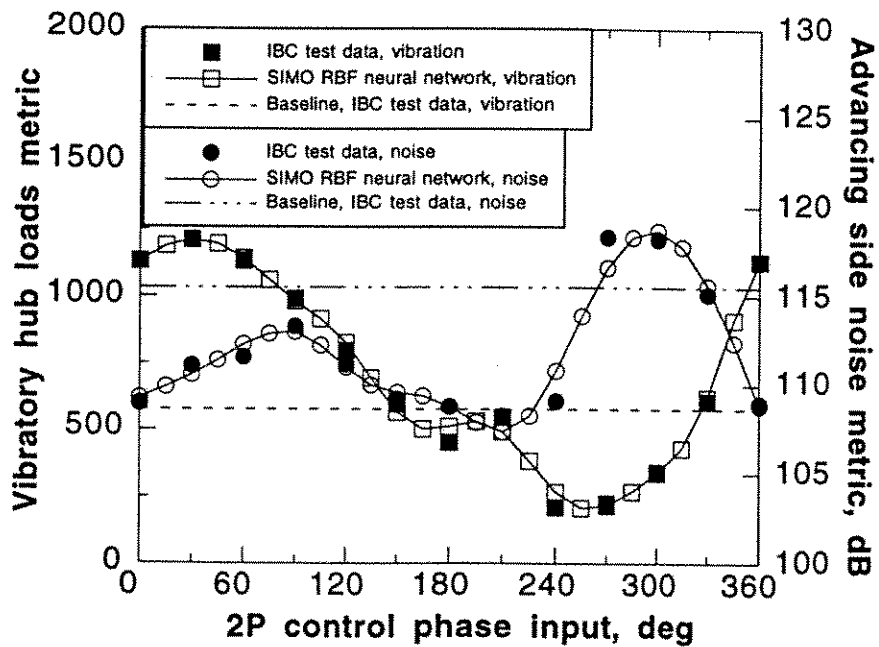
Fig. 13. Case 2 (Noise and Hub Loads Control), noise and hub loads metrics.
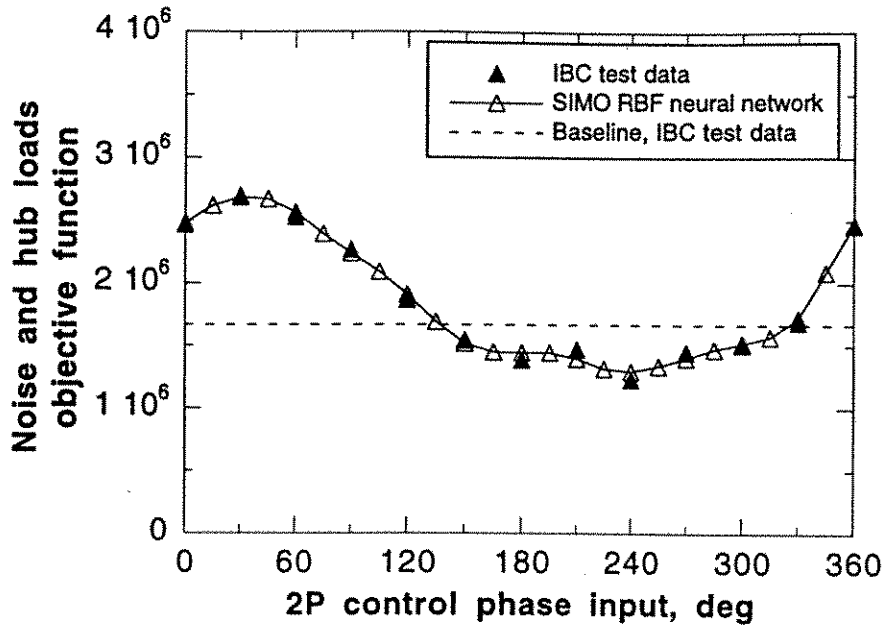
Fig. 14   Case 2 (Noise and Hub Loads Control), noise and hub loads
objective function.
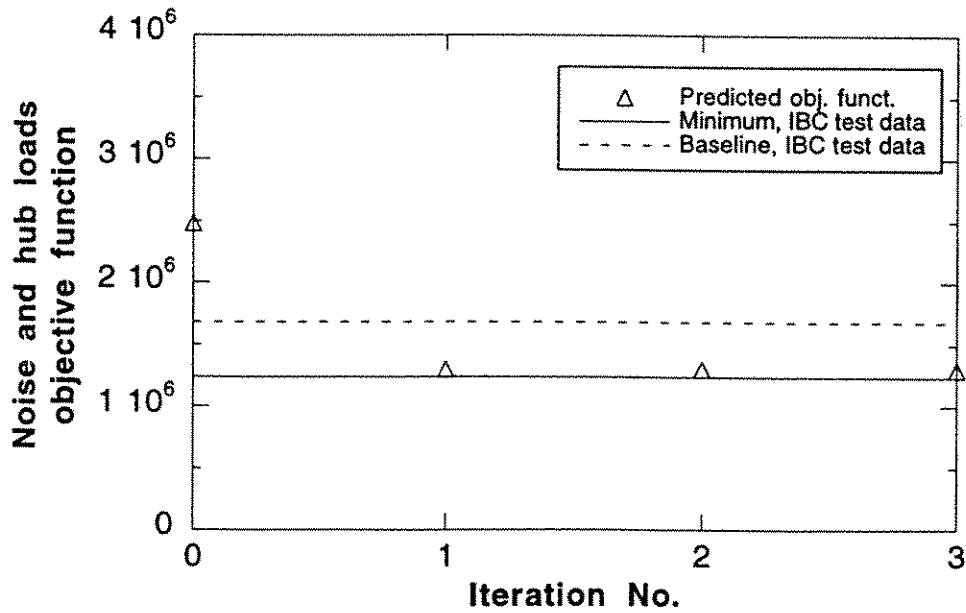
Fig. 15a. Case 2   (Noise and Hub Loads Control), convergence of
objective function J (simultaneous neural control of noise and hub
loads).
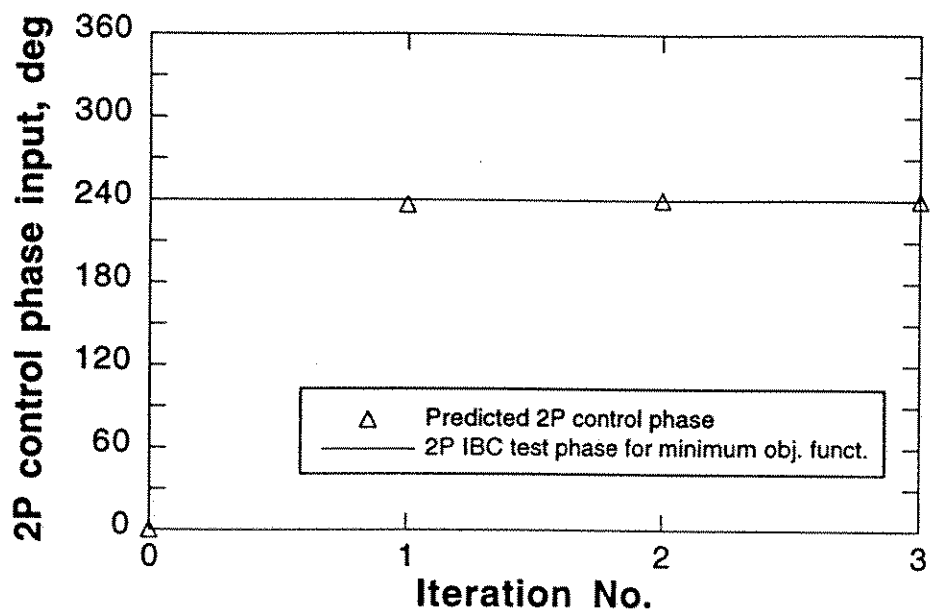
Fig. 15b   Case 2   (Noise and Hub Loads Control), convergence of 2P control phase input (simultaneous neural control of noise and hub loads, see Fig. 15a also).
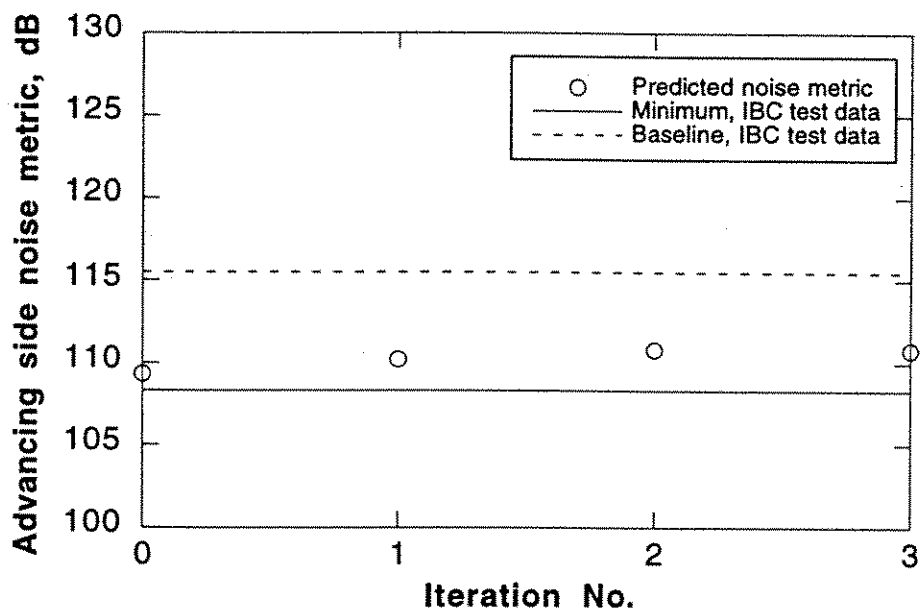
Fig. 16a. Case 2 (Noise and Hub Loads Control), convergence of noise metric ASNM (neural control of noise and hub loads)
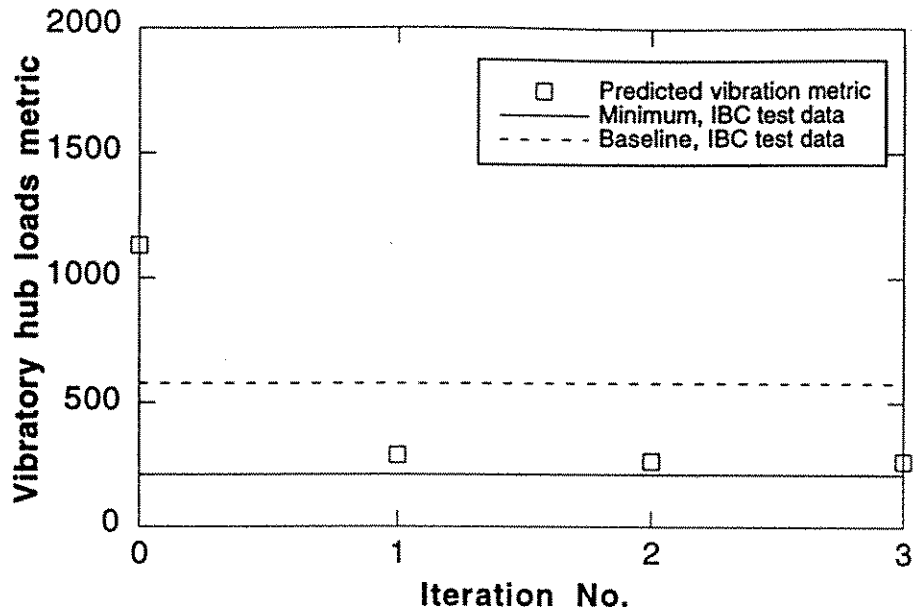
Fig. 16b. Case 2 (Noise and Hub Loads Control), convergence of hub loads metric VHLM (simultaneous neural control of noise and hub loads).
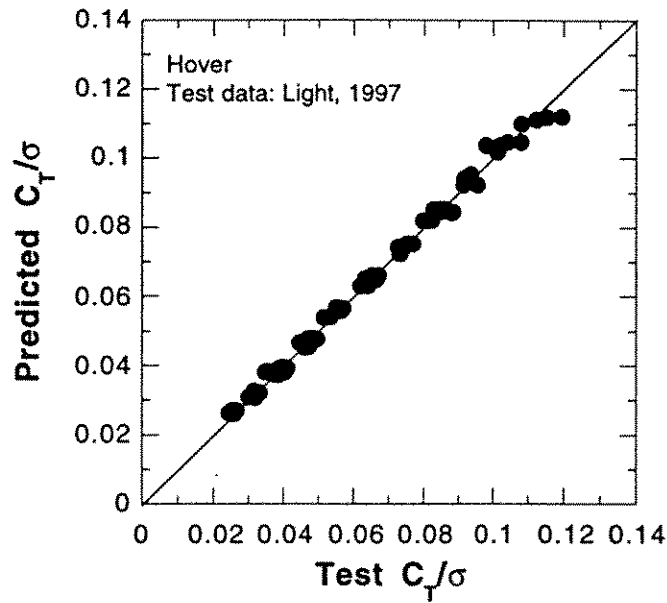
Fig. 17 Measured inputs: C_T/σ correlation
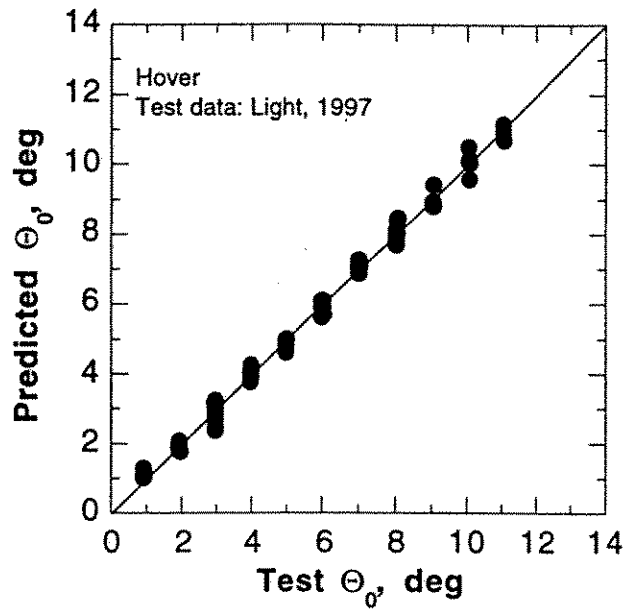
Fig. 18   Derived inputs: collective correlation
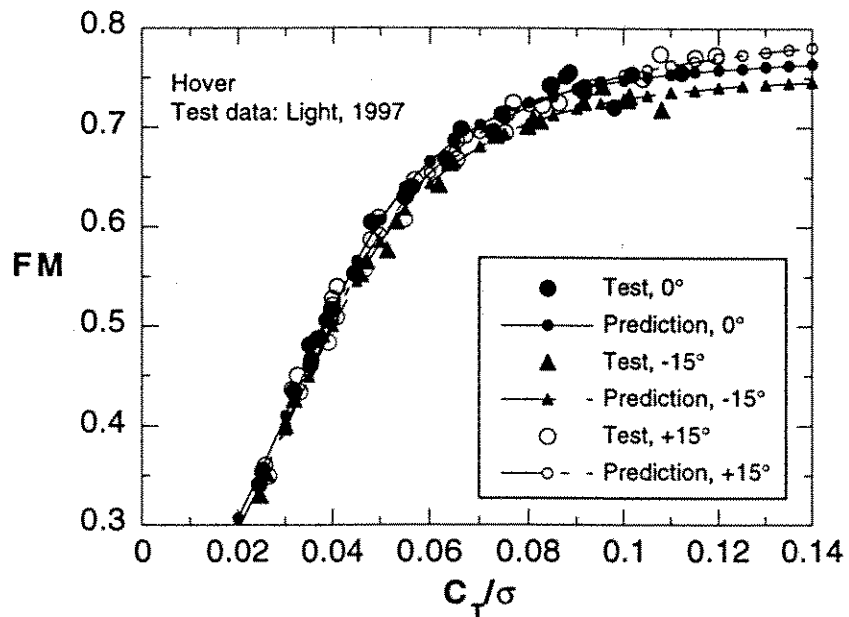
Fig. 19   Figure of merit variation with C_T/σ: 3 SISO neural network fits
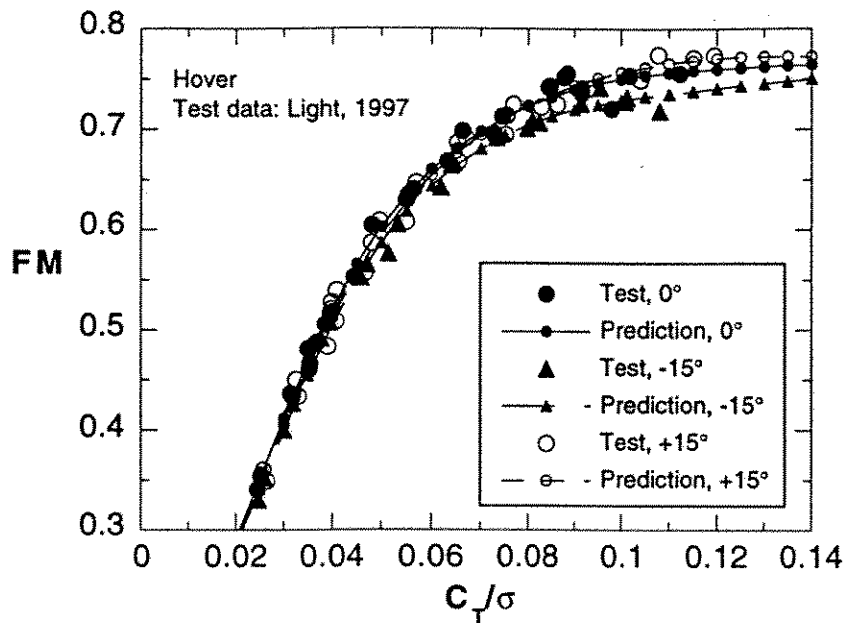
Fig. 20   Figure of merit variation with C_T/σ: MIMO neural network fit
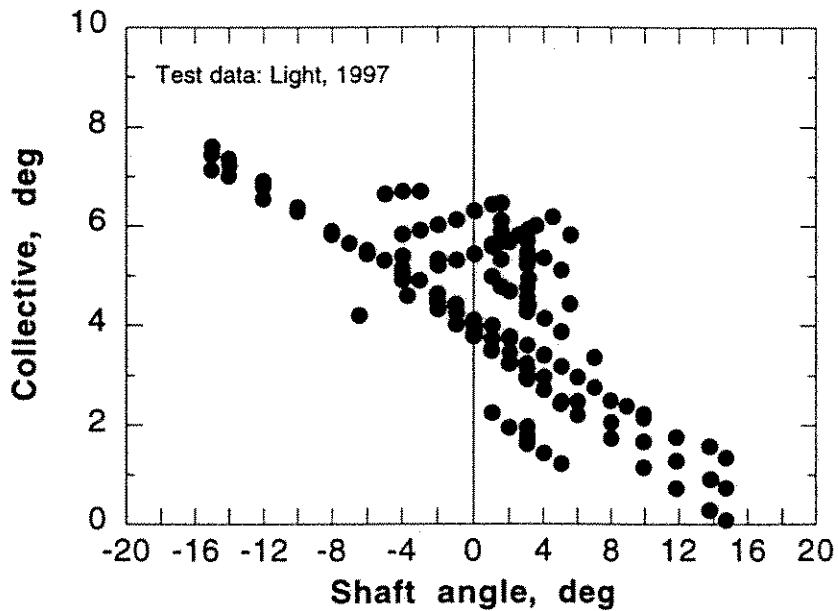
Fig. 21   Wind tunnel test data: collective versus α_s (varying μ and C_T/σ), forward flight
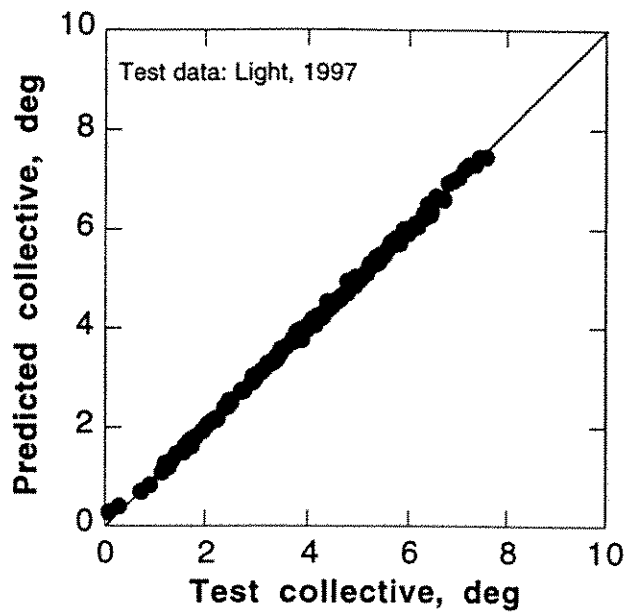
Fig. 22 Forward flight collective correlation: MIMO back-propagation neural network
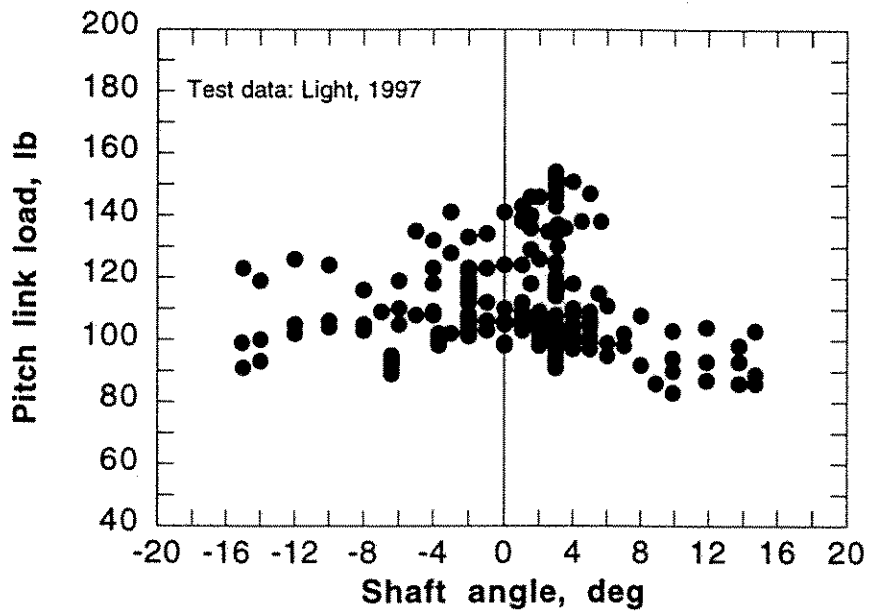
Fig. 23 Wind tunnel test data: oscillatory pitch link load versus α, (varying μ and C_T/σ), forward flight
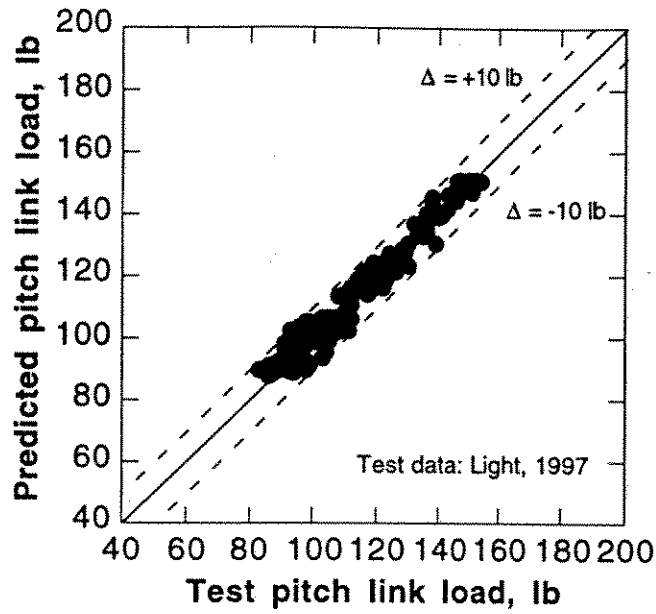
Fig. 24 Forward flight oscillatory-pitch-link-load correlation: MIMO neural network
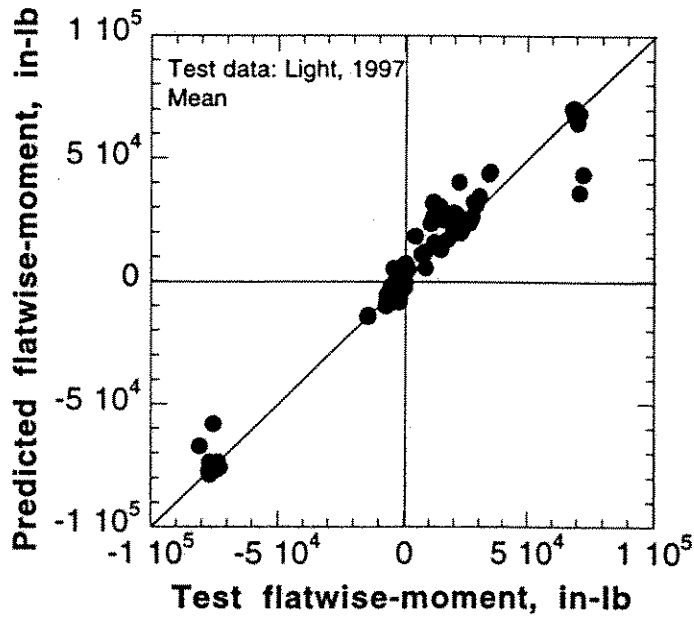
Fig. 25 Forward flight mean flatwise moment correlation: MIMO neural network
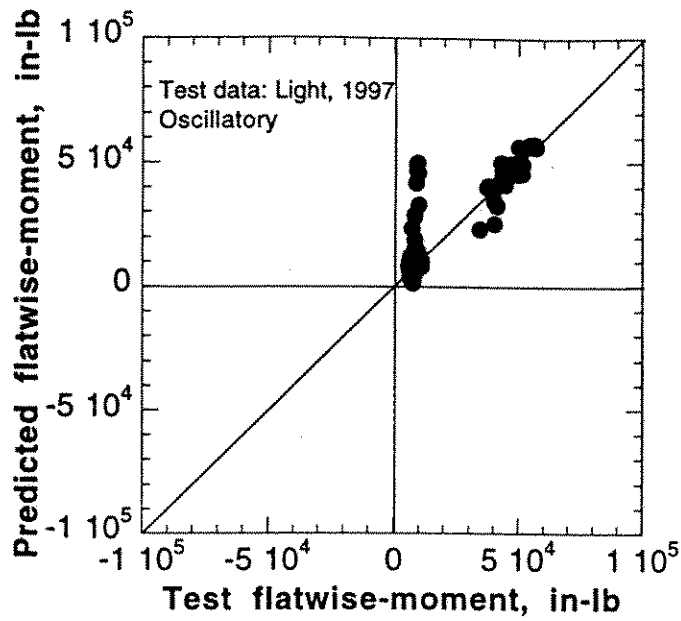
Fig. 26 Forward flight oscillatory flatwise moment correlation: MIMO neural network
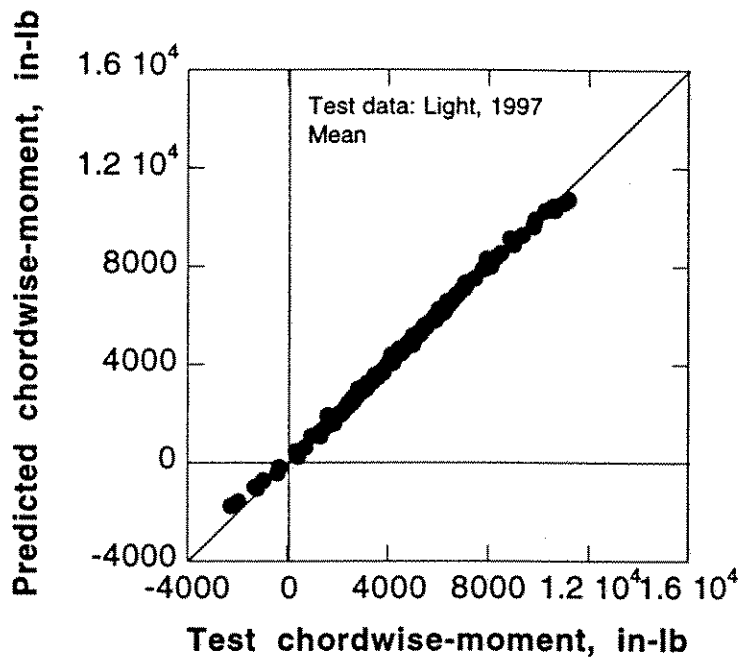
Fig. 27 Forward flight mean chordwise moment correlation: MIMO neural network
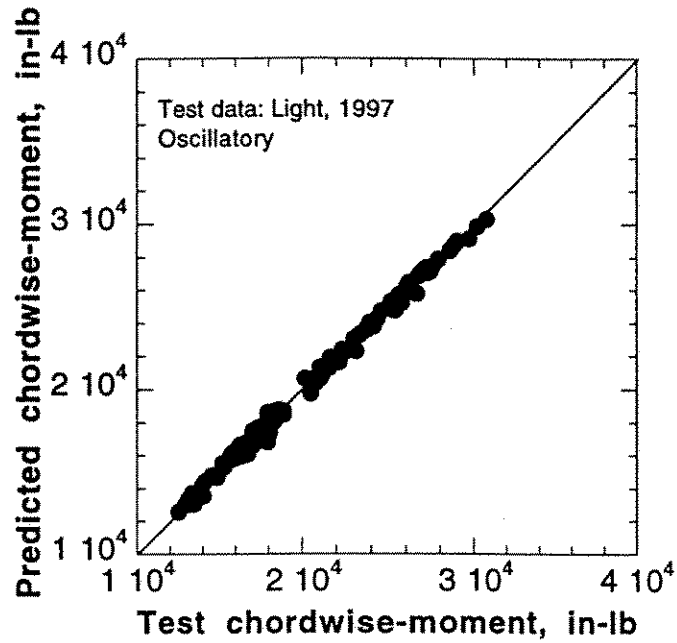
Fig. 28   Forward flight oscillatory chordwise moment correlation: MIMO neural network
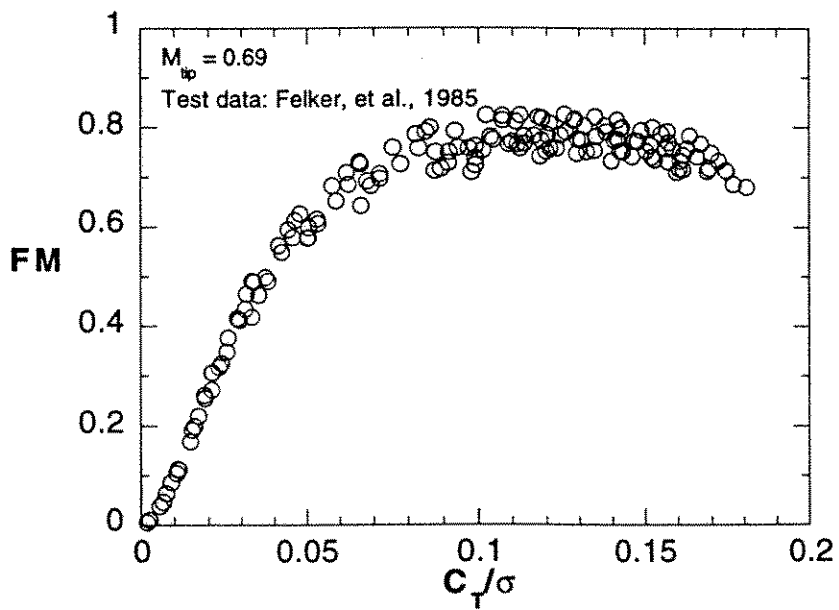
Fig. 29 Outdoor test data, "all winds"
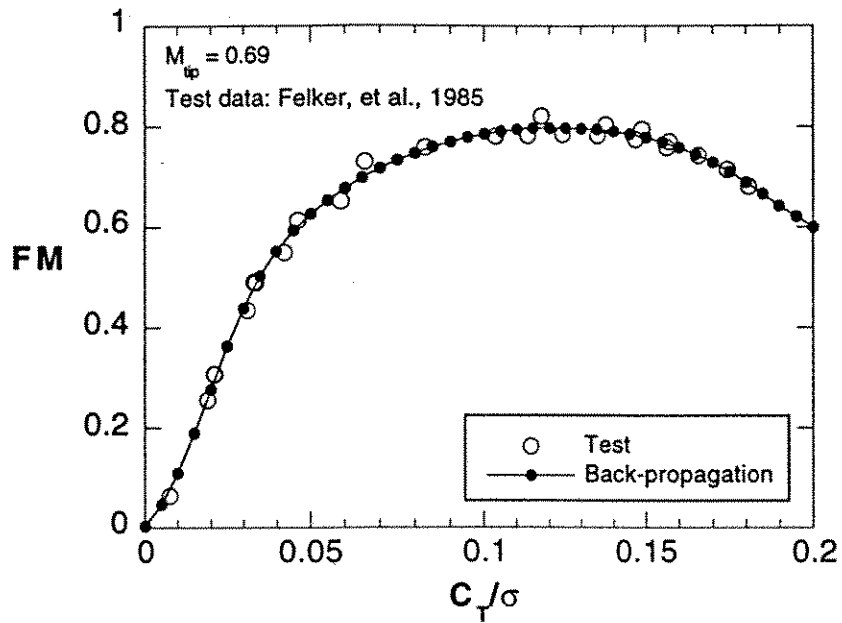
Fig. 30   Outdoor "zero wind" representation (SIMO neural network), winds < 0.5 m/s
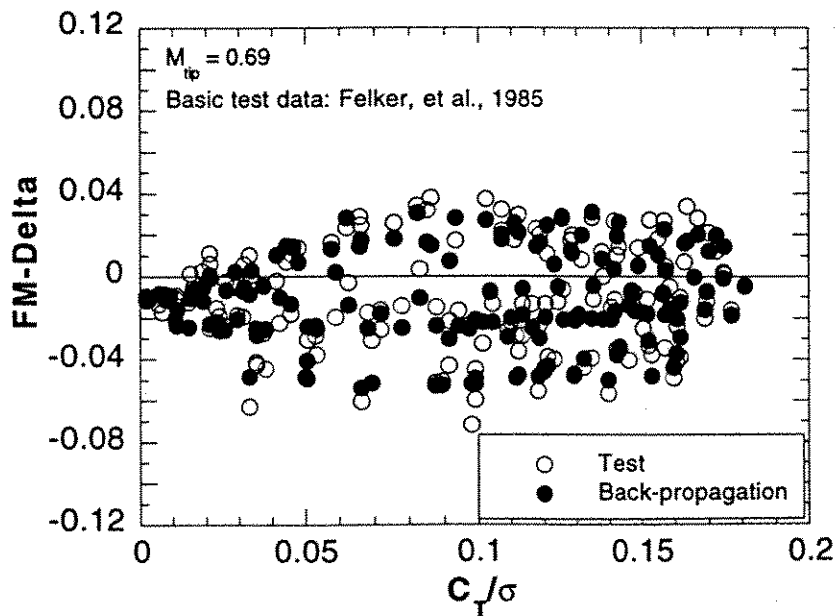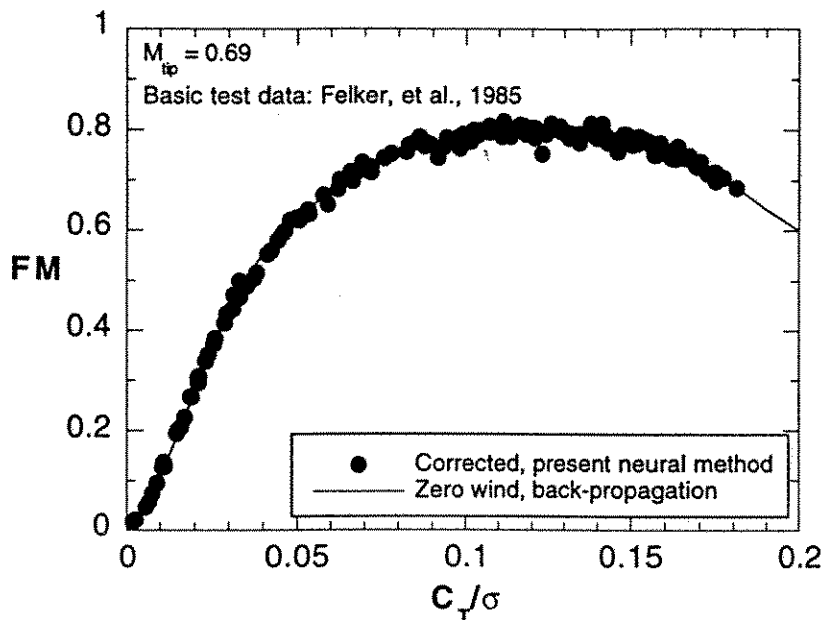
Fig. 31   Test and MISO neural-network-predicted FM-deltas

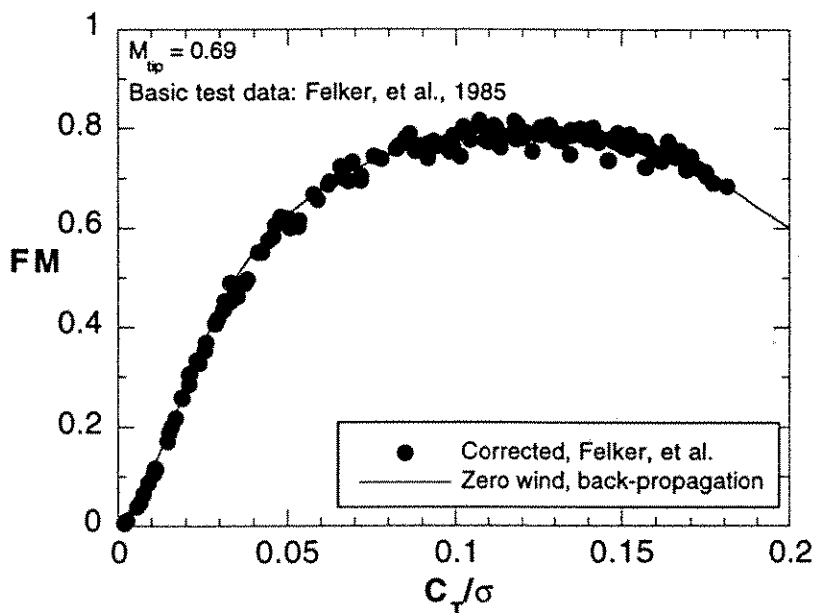Fig. 32 Present neural-network-corrected figure of merit

Fig. 33   Felker's momentum-theory-based corrected figure of
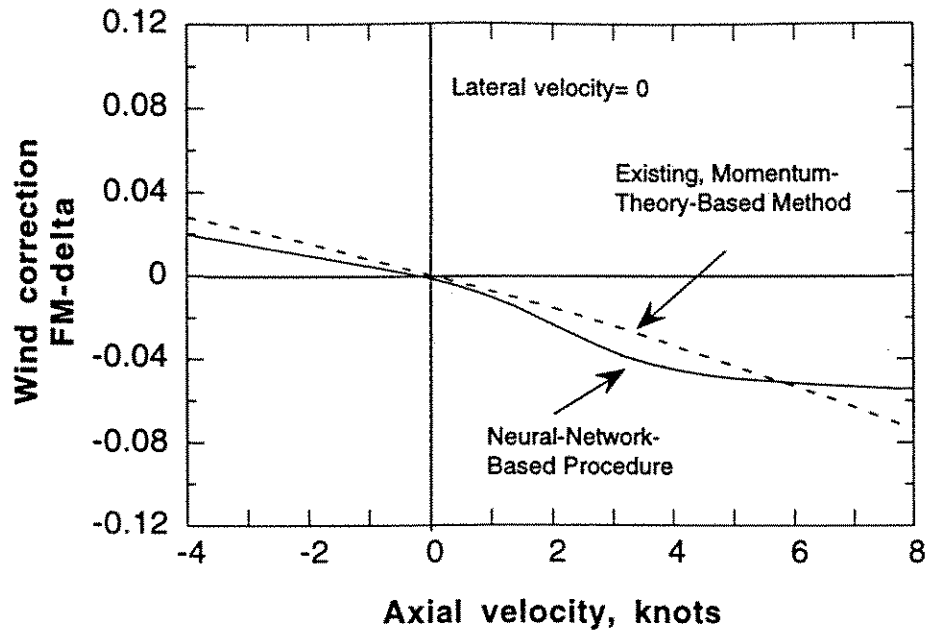merit

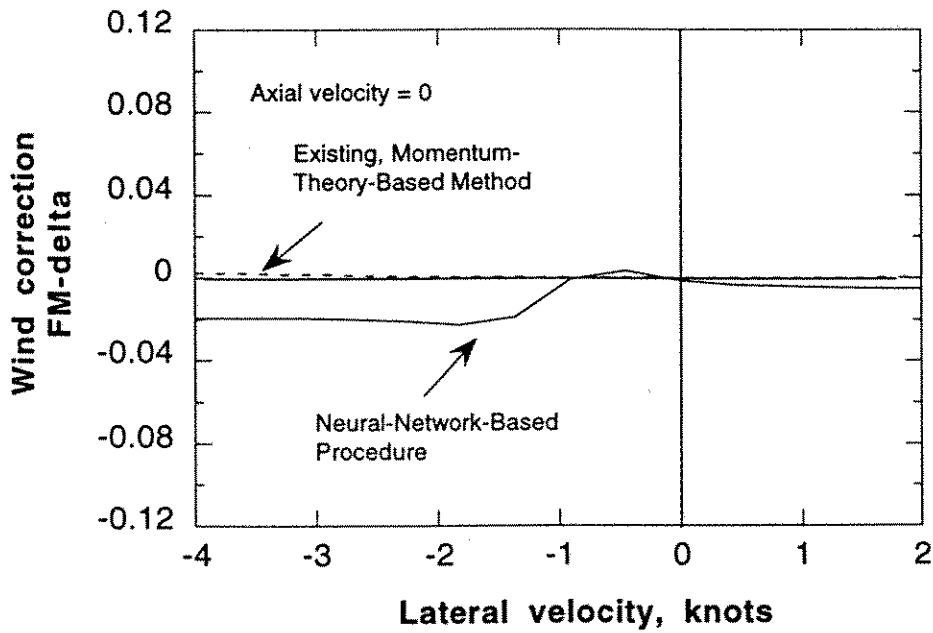Fig. 34 Outdoor, hover (example): axial velocity effect, lateral velocity zero

Fig. 35 Outdoor, hover (example): lateral velocity effect, axial velocity zero